Renewable and Sustainable Energy Reviews 16 (2012) 1588–1610

Contents lists available at SciVerse ScienceDirect

Renewable and Sustainable Energy Reviews

journal homepage: www.elsevier.com/locate/rser

Modeling HCCI combustion of biofuels: A review

N.P. Komninos*, C.D. Rakopoulos

Internal Combustion Engines Laboratory, Thermal Engineering Department, School of Mechanical Engineering, National Technical University of Athens, 9 Heroon Polytechniou St., Zografou Campus, 15780 Athens, Greece

ARTICLE INFO

Article history:
Received 8 November 2011
Accepted 25 November 2011
Available online 18 January 2012

Keywords:
Biofuels
HCCI
Simulation
Ethanol
Hydrogen
DME
DEE
Biodiesel
Methyl butanoate
Methyl decanoate

ABSTRACT

The ever increasing energy demands coupled with the limited availability of fossil fuels and the detrimental environmental effects resulting from their use, has guided research toward seeking alternative fuels to gradually substitute conventional ones. Among these, biofuels have received increasing attention due to their attractive features of being renewable in nature and reducing the net CO_2 emissions. Biofuels have been used in conventional diesel and gasoline engines either as neat fuels or as supplements.

Fortunately, a relatively new combustion concept for internal combustion engines, namely homogeneous charge compression ignition (HCCI) combustion, has been evolved in parallel to the biofuel research. HCCI combustion seems to be able to take advantage of the diverse properties of biofuels, since in this combustion mode ignition is not externally instigated, but relies on the compression and subsequent autoignition of a fuel–air mixture. This fact allows the utilization of different fuels or blends thereof, in order to regulate the ignition point and provide adequate operation under diverse operating conditions.

This study provides an overview of existing simulation models for the simulation of biofueled HCCI combustion. Simulation models aid and supplement the experimental research conducted on HCCI combustion, providing a fundamental insight into the physicochemical parameters affecting performance and emissions formation. The simulation models include single-zone models, multi-zone models, probability based models, and multi-dimensional models in order of complexity. The vast majority of these models implement chemical kinetics to simulate the combustion process, not only due to the inherent dependence of HCCI combustion on the physicochemical properties of the fuel, but also due to the sometimes complex chemical structure of the biofuels, which include esters, ethers and alcohols. The reaction paths for these homologous series are quite different from the conventional hydrocarbons used to simulate conventional fuels, and provide the ground for current and future research work.

Contents

* Corresponding author. Tel.: +30 210 7721710.
E-mail address: nkom@central.ntua.gr (N.P. Komninos).

1364-0321/$ – see front matter © 2011 Elsevier Ltd. All rights reserved.
doi:10.1016/j.rser.2011.11.026

Nomenclature

B	cylinder bore (m)
h	molar specific enthalpy (J/kmol)
i	any zone
k	species index
K	number of species
n	moles
P	pressure (N/m^2)
S	cylinder height (m)
T	temperature (K)
t	thickness (m)
U	internal energy (J)
V	volume (m^3)
z	number of zones

Greek symbols

λ	air–fuel equivalence ratio (lambda)
ϕ	fuel–air equivalence ratio (phi)

Subscripts

chem	chemical
cyl	cylinder
HT	heat transfer
i	zone index
in	inlet or initial
w	wall

Superscripts

in	inflow
out	outflow
tr	transferred

Abbreviations

a	after
b	before
BDC	bottom dead center
CA	crank angle
CAD	crank angle degrees
CO	carbon monoxide
CFD	computational fluid dynamics
CI	compression ignition
CR	compression ratio
DI	direct injection
DTBP	di-tertiary butyl peroxide
EDC	eddy dissipation concept
EGR	exhaust gas recirculation
EtOH	ethanol
EU	European union
EVC	exhaust valve closing
EVO	exhaust valve opening
FID	flame ionization detector
HC	(unburned) hydrocarbon(s)
HCCI	homogeneous charge compression ignition
HRR	heat release rate (J/deg)
HTR	high temperature reaction
HTHR	high temperature heat release
IA	injection angle
imep	indicated mean effective pressure (bar)
ISFC	indicated specific fuel consumption (g/kWh)
IT	injection timing
IVC	inlet valve closing
IVO	inlet valve opening
LES	large eddy simulation
LTR	low temperature reactions
LTHR	low temperature heat release
MB	methyl butanoate
MD	methyl decanoate
MeOH	methanol
MON	motor octane number
MRG	methanol reformed gas
MSW	municipal solid waste
MZ	multi-zone
NO_x	nitrogen oxides
NVO	negative valve overlap
OHC	oxygenated (unburned) hydrocarbons
PDF	probability density function
PI	port injection
PRF	primary reference fuel
RES	renewable energy sources
RON	research octane number
SRM	stochastic reactor model
SI	spark ignition
SZ	single-zone
TC	turbocharged
TDC	top dead center
toe	tonnes oil equivalent
UHC	unburned hydrocarbons

1. Introduction

During the last decades two main concerns have arisen in the energy generation and transportation sectors, namely the increasing energy demand coupled with the limited availability of oil reserves and the detrimental environmental effect produced by their exploitation to deliver energy and motion. Nuclear energy could be used to gradually displace fossil fuel based energy production, but the late accident in the Fukushima nuclear power plant has raised many concerns related to the hazards of nuclear power plants; it seems that the efforts toward the establishment and the public acceptance of nuclear energy have yielded somewhat to skepticism. In an effort to gradually displace fossil fuels, gross inland energy consumption[1] of renewable energy sources (RES) has increased in the European Union (27 countries) in the decade 1999–2009 from over 5% to approximately 9% [1]. However, this increase in the share of renewable energy consumption seems to be mainly due to the reduction in the solid fuel energy consumption share, since the nuclear energy consumption share (~13–14%) and the combined share of petroleum and natural gas (~61%) have remained fairly constant (Fig. 1).

The use of fossil fuels has increased the energy dependence of many countries around the world, since oil production is extremely localized with the Middle East possessing over 55% of the proved oil reserves world wide as of 2009 [2,3]. This impacts all countries and citizens around the world, since the oil prices are reflected on virtually every commodity. Moreover, it creates and sustains energy insecurity among countries with high energy dependence.

Another detrimental effect of the use of fossil fuels is related to the environmental impact from their use for energy production and transportation. The fuel combustion in internal combustion engines produces – among others – CO_2, a major greenhouse gas that is

[1] Gross inland energy consumption refers to the total energy demand of a country or region. It covers energy consumption by the energy sector itself, distribution and transformation losses, final energy consumption by end-users and statistical differences. It does not include energy provided to maritime bunkers [1].

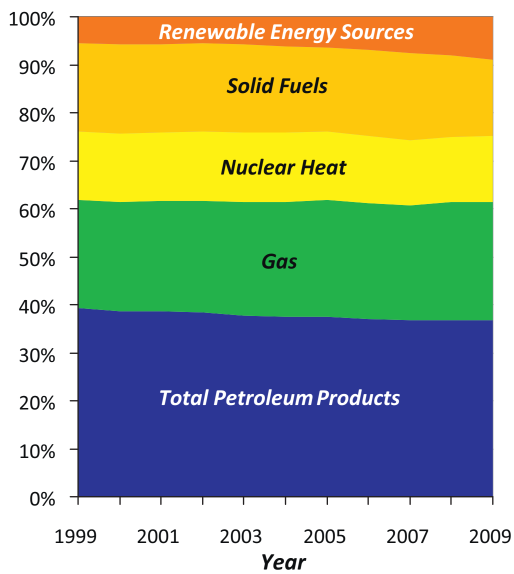


Fig. 1. Gross inland energy consumption share by fuel in the EU (27 countries). Gas: almost exclusively natural gas. Renewable energy sources: biomass and renewable wastes, hydro, geothermal, wind, solar, wave, tide and ocean energy.
Data source: Eurostat (online data codes: nrg_100a, nrg101a, nrg_102a, nrg_103a, nrg_104a, nrg_1071a) [1].

known to contribute to the global warming effect. The main issue is not the production of CO_2 itself, since the combustion of most fuels leads to its production, but the fact that in the case of fossil fuels the CO_2 emitted cannot be reconverted to the original fuel by any short-term, natural – and therefore energy neutral – process.

In view of the first issues analyzed, i.e. the energy dependence of most of the countries, the instability of the oil prices and the increasing demand of fossil fuel energy, alternative fuels have been sought after. Among those, biofuels have received increasing attention due to their additional attribute of being renewable. The term "biofuel" refers to any fuel that can be produced from biomass, such as starch, sugars, lignocellulosic material, animal fat, oleaginous plants, etc. The main advantage of a biofuel is that it can be reconstructed by natural processes using the CO_2 emitted from its combustion. This is part of the photosynthetic process of the plants, which use sunlight and CO_2 to build their cells. Thus, biofuels have the potential to be CO_2 neutral. This is depicted in Fig. 2, in which a comparison is made between the biofuel energy system and the fossil fuel energy system.

Initially, feedstock such as barley, wheat, corn, sugar beat, sugarcane, etc. was – and still is – used for ethanol production; oleaginous plants such as soybeans, castor beans, rapeseed, Jatropha and palm were used for biodiesel production. However, the feedstock utilized for the production of these "first generation" biofuels originates from edible crops. This led to an unfavorable effect related to food security in terms of both land use and food prices. With over 1/8th of the population worldwide undernourished as estimated in 2010 [5,6], using part of the edible crops to produce biofuels did not seem a socially just choice. Added to the land use was the issue of rising food prices due to the increased demand, which was instigated by the alternative use of food commodities for fuel production [2].

The food security issue raised concerns related to the choice of biofuel production routes and shifted research toward biofuel production from non-edible feedstock, mainly lignocellulosic material or "plant biomass". The term "second generation" biofuels is used to depict this shift in the feedstock used, but not the final fuels produced. The lignocellulosic material is abundant in plants and mainly consists of polysaccharides [7]; biofuels can be obtained from this feedstock by hydrolysis and fermentation, for ethanol production, and by gasification to produce liquid hydrocarbons, biodiesel, bioDME and bio Synthetic Gas. Additionally, algae seem a promising feedstock for the production of second generation biofuels and especially diesel fuel. Their advantages are their high growth rates, tolerance to diverse environmental conditions, high CO_2 trapping and fixation ability, high oil content – sometimes exceeding 80% of their dry weight – and the high microalgae yield per hectare, which is almost an order of magnitude higher than the palm oil yield [7]. Owing to the fact that other non-fuel products can also be obtained from biomass, an integrated approach is being researched to fully exploit the biomass available and produce all possible products from biomass, including biofuels and a platform of chemicals, in biorefinery systems [4,7]. The production of second generation biofuels is not yet cost effective since there are a lot of technical barriers to be overcome [7].

In view of the attractive attributes of biofuels, efforts have been made to introduce them into the energy consumption systems. In Fig. 3 the final energy consumption[2] of RES in EU is shown for the year 2009. It can be seen that the main sector in which biofuels – especially liquid ones – are currently used, is the transport sector and particularly road transports. Fig. 3 also indicates that liquid biofuels – including bioethanol, biomethanol, biodiesel, bioDME and other – are currently the gateway for the penetration of RES into the transport sector. The share of liquid biofuels in the transport sector and especially road transports has increased during the last decade as shown in Fig. 4.

These data highlight the importance of biofuels and justify the research effort toward their utilization in conventional (CI and SI) engines as well as in Homogeneous Charge Compression Ignition (HCCI) engines. In Diesel engines fuels such as n-butanol, ethanol, biodiesel, DME, either neat or in blends, have been tested and/or simulated [8–16]. Some of these biofuels, such as esters and DME, have an inherent tendency to reduce soot formation due to their chemical structure; the tendency to form soot precursors decreases as the oxygen content in the fuel molecule increases and/or the number of C–C bonds decreases [16]. This is due to the fact that the oxygen bound carbon atoms tend to form CO or CO_2 rather than participate in soot formation reactions [17]. In spark ignition engines hydrogen, biogas, ethanol, DME have been tested and/or simulated [18–21].

Apart from the conventional combustion modes a relatively new concept has been developing during the last two decades, i.e. homogeneous charge compression ignition combustion (HCCI). In HCCI combustion a mixture of fuel and air is introduced into the combustion chamber early during compression or during the intake stroke. The mixture is compressed and autoignites at the point where the local thermo- and fluid-dynamic conditions are favorable [22]. The main advantage of the HCCI concept relative to conventional combustion modes is the significant reduction of NO_x emissions and the absence of soot in the exhaust. Moreover, the fast combustion usually encountered and the unthrottled operation are prone to yield high indicated thermal efficiency. However, HC and CO emissions are usually high due to bulk quenching at low loads, and wall quenching and crevice flows at higher loads [23].

Added to these unfavorable attributes of HCCI is the inability to directly control the combustion phasing in HCCI engines. This is a major obstacle preventing the implementation of the HCCI concept. HCCI ignition relies heavily on chemical kinetics and largely depends on the fuel used. In an effort to control ignition and the combustion rate, thereby expanding the HCCI operation over a wide range of load–engine speed, various means have been used, such as variable compression ratio, variable valve timing, variable inlet

[2] Final energy consumption is the total energy consumed by the end-users, such as industry, transports, households, services, etc. [1].

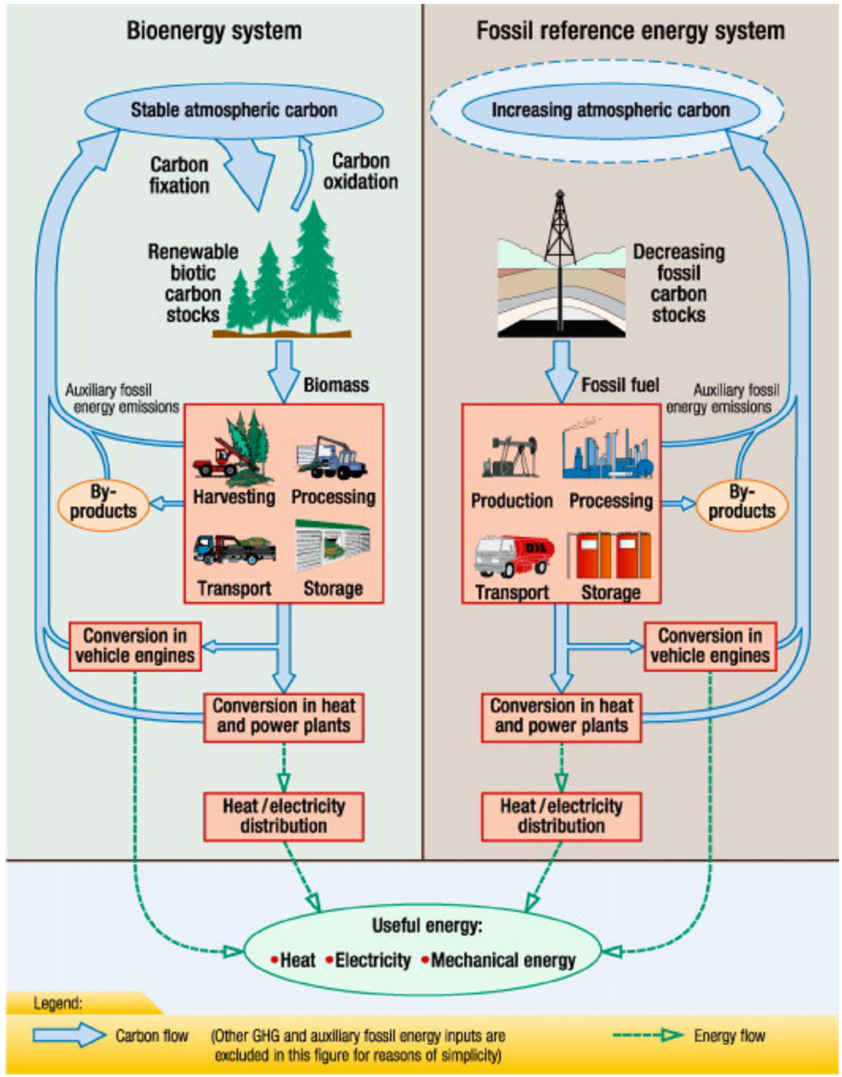


Fig. 2. Comparison of bioenergy and fossil fuel energy systems [4].

temperature, internal or external EGR, direct fuel injection, etc. [23]. A promising method for the combustion control seems to be the use of alternative fuels and fuel blends, depending on the characteristics of the engine (compression ratio, etc.) and the operating conditions [23–25]. The main concept is that fuels with different autoignition tendencies can be blended at varying proportions to regulate the ignition point at various load–speed regions [26]. This is a fortunate evolution since the fuels used in the blends may

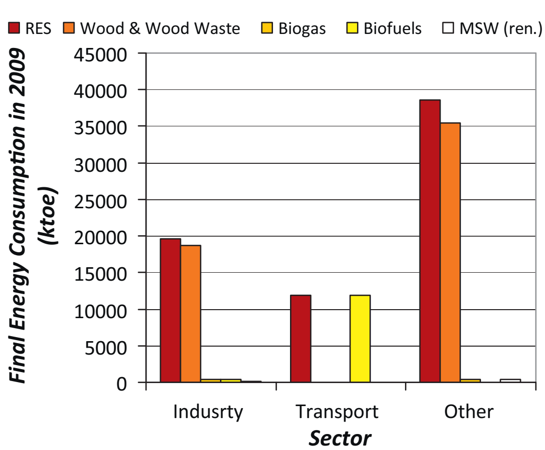


Fig. 3. Final energy consumption of RES, biomass and renewable wastes by sector in the EU (27 countries) in 2009. MSW (ren.): municipal solid waste (renewable).
Data source: Eurostat (online data codes: nrg_1071a, nrg_1073a) [1].

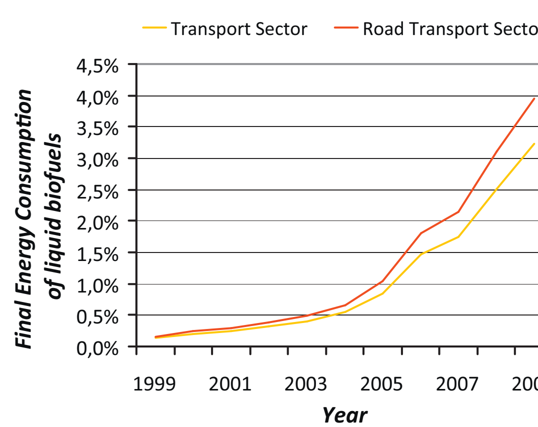


Fig. 4. Final energy consumption share of liquid biofuels in the transport sector and the road transport sector in the EU (27 countries).
Data source: Eurostat (online data codes: nrg_100a, nrg_1073a) [1].

as well be biofuels. Thus, hydrogen [27], ethanol [28–32], ethers [33–37] and biodiesel [38] have been used in HCCI engines, either as neat fuels or in blends. High cetane number fuels (such as DME) can be used as ignition promoters in the blend and high octane number fuels (e.g. ethanol, methanol, etc.) can be used as ignition suppressors. With the use of closed or open loop control systems, the resulting fuel blend can provide the means to control HCCI ignition over a wider range than the one provided by the individual neat fuels [25]. This has already been demonstrated in HCCI engines using blends of n-heptane and isooctane [26].

As is the case with conventional combustion types (SI and CI), the HCCI combustion mode can be studied using simulation models of various degrees of complexity. Simulation models describe the fundamental processes occurring within the combustion chamber and – if accurate enough – can help toward understanding the effects of individual operating parameters on HCCI combustion. Such an analysis is not always feasible in experiments, since it is usually difficult to isolate the effect of a single parameter – be it fuel properties, inlet conditions, etc. – without directly or indirectly affecting another parameter. Simulation models can provide insight into the fundamental processes occurring during combustion and/or during the stage of gas exchange processes, depending on the sophistication level of the model. Features such as combustion chemistry, heat and mass transfer can be studied so that the crucial factors affecting them can be assessed. Especially in the case of biofuels, which have not been numerically studied extensively until recently, there is a lot to be explored as regards combustion chemistry, emissions formation, transport properties, etc. Combustion chemistry affects significantly the mixture autoignition, combustion rate and emissions formation. Transport properties affect heat and mass transfer within the combustion chamber, which determine the temperature field or temperature–mass distribution within the combustion chamber. Moreover, in the case of direct injection HCCI, in which the fuel is directly injected into the combustion chamber, the fuel transport properties must be adequately modeled to simulate the formation, break-up, vaporization and mixing of the fuel jet with the air. Such phenomena determine the mixture stratification and the possibility of fuel jet impingement on the combustion chamber walls.

HCCI simulation models are divided into single-zone, multi-zone and computational fluid dynamics (CFD) models, in order of increasing complexity. In single-zone models the main assumption is the uniformity of the charge properties within the combustion chamber. Multi-zone models consider multiple regions within the combustion chamber, each of which is considered an open thermodynamic system of uniform properties. CFD models are the most sophisticated ones, providing detailed description of the in-cylinder gas motion and thermodynamic state on a local level. However, this increased level of sophistication is not without compensation, in terms of increased computational time and effort.

In the following sections single-zone, multi-zone and CFD models, which have been constructed for biofueled HCCI combustion are presented. Since the vast majority of HCCI simulation models use chemical mechanisms of various levels of detail to describe the chemical kinetics of the ignition and combustion processes, a separate section is devoted to the use of chemical kinetics. The HCCI simulation models presented in the following sections are included in this study regardless of whether they produced specific biofueled-oriented results. The selection criteria were considered satisfied by the mere fact that biofueled HCCI combustion was simulated. Upon consideration of the relatively short simulation history of the HCCI engine, simulation data for biofueled HCCI engines have their own obvious merits and provide a reference for future studies nonetheless.

2. Chemical kinetics modeling – reaction pathways

Almost all of the simulation models used in HCCI combustion modeling and all simulation models presented herein include chemical kinetics. This is the result of the decisive role chemical kinetics play in HCCI combustion. Since no external means are utilized to instigate ignition, the latter relies on the reaction kinetics of the fuel. Ignition commences where the thermodynamic conditions of pressure, temperature and species concentration are favorable. Moreover, the specific characteristics of the reaction paths and intermediate species also affect the formation of pollutants such as NO_x, CO and unburned HC. These issues provide the momentum for the ongoing research oriented toward building chemical reaction paths, which are able to describe in various levels of detail the oxidation characteristics of fuel–air mixtures under various operating conditions. Compared to the diversity of the biofuels used, which include hydrogen, alcohols, ethers and esters, the chemical mechanism research has a short history. The difficulties encountered involve the identification of the primary and secondary reaction pathways as well as the reduction of the resulting chemical mechanisms. This reduction is paramount if the chemical mechanisms are to be used in simulation models, since the simulation time increases non-linearly with the increase of species and reactions. Such considerations are especially important when using the chemical mechanisms in CFD models, in which the computational time cost is already aggravated by the solution of the Navier–Stokes equations.

As regards the chemical mechanisms used in modeling HCCI combustion, care should be exercised during the choice of the specific mechanism, since the various existing mechanisms do not necessarily provide similar results even for well-known fuels such as isooctane [39]. Therefore, comparisons of ignition timings and global combustion rates must be interpreted with caution, especially when differences between fuels are assessed [40]. This also holds true for the comparison of NO_x emissions, which are known to be sensitive to peak temperature variations and consequently to the ignition timing predictions. Thus, it is essential for the researcher to investigate the conditions under which the mechanisms were developed and the experiments used for their validation (shock tube, flow reactor, jet stirred reactor, rapid compression machine, laminar flame, HCCI engine, etc.). Preferably, the mechanisms have to be validated at low equivalence ratio and high pressure since these conditions are relevant to HCCI combustion in engines [39]. Furthermore, it has to be kept in mind that the fuel oxidation chemical mechanisms usually refer to surrogates of actual fuels, which cannot describe in exhaustive detail all the actual fuel properties. It is obvious that even the detailed mechanisms have their limitations and their validation cannot be exhaustive, considering the diverse operating conditions encountered in HCCI engines (high EGR dilution, fuel injection in hot residuals during negative valve overlap HCCI, etc.).

Table 1 includes chemical reaction mechanisms for various biofuels found in the literature. Some of these mechanisms have not been used in the simulation studies presented herein, but are available for future research. However, the vast majority of the oxidation mechanisms included in Table 1 has been implemented in simulation models, which are described in detail in the subsequent sections. The citations describing each mechanism have been numbered consecutively, while the citations of the papers in which these mechanisms were used have been numbered in order of appearance in the text.

3. Single-zone modeling

Single-zone models are often used in HCCI modeling due to the short computational time required for the simulation. In the

Table 1
Available reaction mechanisms for biofuel combustion simulation.

#	Number of species/number of reactions	Source Ref.	Used in Ref.[a]	NO_x[b]	Fuel	Simul. model	Engine type[c]	CR	P_{in}[d] (bar)	T_{in}[d] (K)	Load (ϕ)[e]	Engine speed (rpm)	Validation[f]	Comments
1-Butanol (BuOH)														
1.	181/1703 and 573/2701	Dagaut et al. [41]	–											w n-heptane
2.	234/1399	Black et al. [42]	–											
3.	251/1990	Dagaut and Togbé [43]	–											w gasoline sur.
4.	1046/4398	Saisirirat et al. [44]	Saisirirat et al. [100]	–	BuOH/n-heptane	SZ	4S	16	–	353	0.3	1500	QLT	63% n-heptane 37% BuOH (vol.)
Diethyl ether (DEE)														
5.	112/484 (+DME, EtOH)	Mack et al. [45]	Mack et al. [45]		DEE/EtOH/DTBP	SZ	4S	16.25	1.7	380–455	0.3	1800	QLT	
6.	215/1051	Yasunaga et al. [46]	–											
Dimethyl ether (DME)														
7.	23/23	Yamada [47]	–											
8.	26/28	Yao et al. [48], Liang et al. [49]	Huang et al. [138]	–	DME	CFD	4S	17.0	1.1	375	0.01–0.14	1400	QNT	
9.	27/35 (+MeOH) 30/44 (+MeOH + NO_x)	Liang [50]	Chen et al. [133]	[82]	DME–MeOH	CFD	4S	17.5	1.02	375–380	0.224, 0.226, 0.605	1400	QNT	DME PI, MeOH DI.
			Yao et al. [137]	–	DME/MeOH	CFD	4S	17.0	1.16	375.6	0.238–0.5	1400	QNT	
10.	28/45	Kim et al. [51]	–											
11.	78/336	Curran et al. [52]	Mack et al. [45]											See DEE
			Yao et al. [48]	–	DME	SZ	4S	17	1	348	0.215, 0.095	1400	QNT	
			Mack et al. [101]	–	DEE/EtOH	SZ	4S	16.25	1.7	–	0.3, 0.4	1800	QLT	
			Yao et al. [103]	–	DME/MeOH	SZ	4S	17	1	350	ϕ_{DME} – 0.17 ϕ_{MeOH} – 0.063	1400	QNT	
			Yao et al. [104]	–	DME/CH_4	SZ	4S	17	1	348	0.297	1400	No	
			Ogawa et al. [105]	–	$DME/MeOH–H_2O–EtOH–H_2–CH_4$	SZ	4S	18.8	1	293	0.16, 0.25	1200	No	
			Yamada et al. [108]	–	$DME/MeOH–O_3$	SZ	4S	8	1	378–388	0.12–0.42 (ϕ_{DME})	600	QNT	
12.	79/351	Fischer et al. [53], Curran et al. [54], Kaiser et al. [55]	Hoffman and Abraham [97]	[83,84]	DME	SZ	4S	16	1.07–1.49	300	0.4	2300	No	
			Shudo and Yamada [106], Shudo et al. [107]	–	DME/H_2	SZ	4S	9.7	–	Ambient	0.27–0.35	1000	QLT	
			Kim et al. [120]	[84]	DME	CFD	4S	17.8		320	8 mg/stroke	1500	QNT	IT 80°–0° bTDC
			Park [139]	[84]	DME	CFD	4S	17.8	1–3	300–460	0.2–2.0	1500	No	
			Kong [142]	[84]	DME/MeOH	CFD	4S	17.7	1.1	340	0.175–0.435	960	QNT	
13.	97/457 (Detailed) 36/73 (Reduced)	Chun-lan et al. [56]	Chun-lan et al. [56]	[85]	DME	CFD	4S	–	1	350	0.214	1500	QNT	Emissions validation

Table 1 (*Continued*)

#	Number of species/number of reactions	Source Ref.	Used in Ref.[a]	NO_x[b]	Fuel	Simul. model	Engine type[c]	CR	P_{in}[d] (bar)	T_{in}[d] (K)	Load (ϕ)[e]	Engine speed (rpm)	Validation[f]	Comments
Ethanol (EtOH)														
14.	38/228	Röhl and Peters [57]	Komninos and Rakopoulos [40]	[86]	EtOH	MZ	4S	21	1	~393	0.1–0.28	994	QNT	
			Komninos and Rakopoulos [113]	[86]	EtOH	MZ	4S	21	1	~393	0.15–0.26	994	QNT	
15.	39/238	Li et al. [58]	Sjoberg and Dec [118]	–	–	–	–	–	–	–	–	–	–	Examined, not used
16.	43/235	Saxena and Williams [59]	Viggiano and Magi [145]	–	EtOH	CFD	4S	21	1	363–393	0.16–0.26	1000	QNT	
17.	57/383	Marinov [60]	Szybist [95]	–	EtOH	SZ	4S	7–29	1	325,500–550	1, ~0.25	900, 2000	No	NVO
			Mack et al. [45]											See DEE
			Ng and Thomson [92]	[84]	EtOH	SZ	4S	15	1	380–660	0.2–0.5	1000	No	EGR, neat EtOH or Reformed
			Martinez-Frias et al. [93]	[84]	EtOH (wet)	SZ	4S	16	3	420 (ivc)	1 (ϕ_{EtOH})	1800	No	TC
			Yang et al. [96]	–	EtOH	SZ	4S	13	–	–	–	1400	No	NVO
			Mack et al. [101]	–	EtOH/DEE	SZ	4S	16.25	1.7	–	0.3, 0.4	1800	QLT	
			Ogawa et al. [105]											See DME
			Komninos and Rakopoulos [113]	[86]	EtOH	MZ	4S	21	1	~393	0.15–0.26	994	QNT	
			Sjoberg and Dec [118]	–	–	–	–	–	–	–	–	–	–	Examined, not used
			Yu et al. [143]	–	EtOH	CFD	4S	17.2	1	354, 400	0.303	1200	QNT	
			Joelsson et al. [144]	–	EtOH	CFD	4S	17.2,17	0.9–1	354, 388	0.303	1200	QNT	
18.	58/310	Curran et al. [61]	Sjoberg and Dec [117]	–	EtOH	MZ	4S	12.8	0.84–1.81	418–443	0.25–0.6	500–2400	QNT	
			Sjoberg and Dec [118]	–	EtOH	MZ	4S	12.8	1	427	0.4	1200	QNT	
19.	112/484	Curran in Mosbach et al. [62]	Mosbach et al. [62]	–	EtOH/DEE	SRM -PDF	4S	16.25	1.18	400–420	0.3, 0.4	1800	QNT	
20.	167/1591, 564/2589	Dagaut and Togbé [63]	–											w n-heptane
21.	235/1866	Dagaut and Togbé [64]	–											w gasoline surr.
22.	1046/4398	Saisirirat et al. [44]	Saisirirat et al. [100]	–	EtOH/n-heptane	SZ	4S	16	–	353	0.3	1500	QLT	63% n-heptane 37% EtOH (vol.)
Ethyl acetate (Ethyl Acet.)														
23.	23/142	Gasnot et al. [65]	Cotino and Jeanmart [150]	–	Ethyl Acet.	CFD	4S	13.3	1.35 boost	462	1.5–4 bar $imep_g$	1200	QNT	Validation with iso-octane
Hydrogen														
24.	10/19	Mueller et al. [66]	–											
25.	10/19	Marinov et al. [67]	Goldsborough and Van Blarigan [89]	–	H_2	SZ	2S	3–38	1.5	300	0.15–0.6	–	No	Free piston engine
			Komninos et al. [112]	[86]	H_2	MZ	4S	18–20	1–2	390–410	0.2–0.4	1000–3000	No	

Table 1 (*Continued*)

#	Number of species/number of reactions	Source Ref.	Used in Ref.[a]	NO_x[b]	Fuel	Simul. model	Engine type[c]	CR	P_{in}[d] (bar)	T_{in}[d] (K)	Load (ϕ)[e]	Engine speed (rpm)	Validation[f]	Comments
26.	11/19	O'Connaire et al. [68]	–											
27.	11/23	Westbrook and Dryer [69]	Noda and Foster [111]	[83]	H_2	MZ	4S	20		345–410	0.1–1.0	1600	No	
28.	11/25	Kee et al. [70]	Fiveland and Assanis [88]	–	H_2	SZ	4S	15	1.2.1.5	400–800	0.15–0.4	1500	No	
29.	12/30	Li and Karim [71], Liu [72]	Liu and Karim [149]	[71,72]	H_2	CFD	4S	16–20	0.85	280–320, 515	0.5	800, 900	QLT	
Methanol (MeOH)														
30.	20/84	Li et al. [73]	–											
31.	22/89	Held and Dryer [74]	Yao et al. [103]											See DME
32.	26/84	Westbrook et al. [75,76]	Ogawa et al. [105]											See DME
33.	52/326	Lindstedt and Meyer [77]	Yang et al. [96]	–	MeOH	SZ	4S	13	–	–	–	1400	No	NVO, 32 Species/167 Reactions
Methyl butanoate (MB)														
34.	41/150 (neat) 53/156 (w n-heptane)	Brakora et al. [78]	Brakora and Reitz [98]	[87]	MB + n-heptane	SZ	4S	18	1.1	300–400	0.298–1.0	1200	No	56 Species/169 Reactions
			Um and Park [152]	[84]	MB + n-heptane	CFD	4S	17.8	1–3 boost	300–460	0.2–2.0	1500	No	
35.	275/1545	Dooley et al. [79]	–											
36.	295/1498	Gaïl et al. [80]	Szybist et al. [38]	[84]	MB + n-heptane	SZ	4S	10.5	1	433–498	0.38–0.48	1800	QNT	T_{in} variable
Methyl decanoate (MD)														
37.	3036/8555	Herbinet et al. [81]	Hofmann and Abraham [97]	[83,84]	MD	SZ	4S	16	1.16–1.65	310, 315	0.4	1670	No	

QLT, qualitative validation-mostly validation of predicted trends; QNT, quantitative validation-includes direct comparison of simulated quantities to experimental measurements; NUM, numerical validation-comparison of the HCCI simulation results using a reduced mechanism against predictions from a detailed mechanism.

[a] The source mechanisms may have been modified for their use in each study. Moreover, some of the mechanisms may have been updated since the publication of each study. Thus, the number of species and reactions are subject to change. Symbol "–" used in this column indicates mechanisms, which are not used in the studies presented herein.

[b] Symbol "–" in NO_x: information not available in the study.

[c] 4S: four stroke engine, 2S: two stroke engine

[d] Subscript "in" refers to inlet or initial conditions

[e] Load is expressed in terms of the fuel–air equivalence ratio, unless explicitly stated otherwise.

[f] Validation refers to the corresponding HCCI simulation model and not to the reaction mechanism(s).

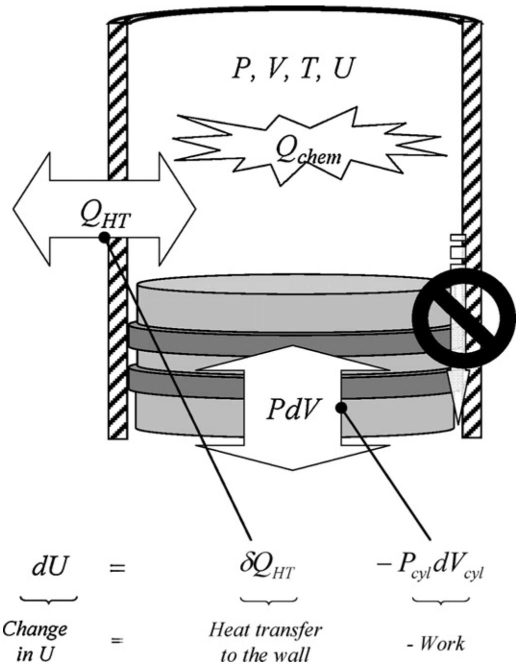


Fig. 5. Schematic of the First Law of Thermodynamics for single-zone models.

single-zone (or zero-dimensional) model the engine cycle is modeled using the First Law of Thermodynamics, taking into account the work absorbed/produced by the piston and – in some cases – the heat exchanged between the charge and the combustion chamber walls, as shown in Fig. 5. Mass blow-by is usually neglected as shown in the figure.

The thermodynamic (pressure, temperature, composition, etc.) and transport properties (viscosity, conductivity, etc.) of the mixture are considered uniform. Since any temperature stratification within the combustion chamber is neglected, the single-zone models tend to overestimate the global heat release rate and, consequently, the pressure rise rate and the maximum combustion pressure. Moreover, since the mixture composition is also considered uniform, the single-zone model is incapable of describing the HC and CO formation processes, unless these are due to global partial combustion of the mixture; under normal HCCI combustion conditions, the formation of these pollutants is believed to occur in the relatively low temperature regions of the combustion chamber as a result of mass transfer between cold and hot regions, in which any HC transferred are partially burned producing CO [23].

Apart from these inherent limitations, single-zone models can be used to provide an estimation of the ignition timing and the formation of NO_x emissions. This is due to the fact that both of these phenomena are primarily controlled by the temperature of the hottest regions of the combustion chamber, which is close to the mean gas temperature of the mixture. Moreover, single-zone models can be used to assess the relative importance of chemical reactions and dominant species that are part of a chemical reaction mechanism describing the fuel–air oxidation. Thus, detailed reaction mechanisms can be compared to reduced ones under the same initial conditions and assumptions provided by the single-zone simulations. The latter features are especially important in the case of biofuels, the combustion chemistry of which is under continuous investigation. The relevant studies are perplexed by the variety of the biofuels, which include organic compounds of diverse homologous series, such as alcohols, ethers, and esters. This is a significant departure from the combustion chemistry of the common pure hydrocarbons, which are usually used as surrogates for the simulation of diesel or gasoline combustion and do not include oxygen atoms in their molecules. Besides the study of the combustion chemistry of neat biofuels, single-zone models can be used to study the characteristics of various fuel blends or the effect of additives on biofuel HCCI combustion. This is an important feature, since the use of fuel blends and additives may provide the means for ignition timing and combustion rate control. Issues like the aforementioned provide the impetus for the ongoing HCCI research [88].

3.1. Hydrogen

Goldsborough and Van Blarigan [89] studied numerically a free-piston hydrogen-fueled HCCI engine. The researchers modeled piston dynamics and the gas exchange process in their free-piston, two-stroke engine. They also used the HCT [90] chemical kinetics software to simulate a zero-dimensional thermodynamic process throughout the engine closed cycle. The hydrogen oxidation was accounted for using the chemical mechanism of Marinov et al. [67]. Heat transfer was accounted for by using Woschni's correlation [91], in which the heat transfer constants were modified to match experimental data from hydrogen combustion in a rapid compression machine. It was found that the engine operation was significantly dependent on the scavenging process, which altered the amount of fuel–air mixture trapped within the combustion chamber, the initial temperature of the charge, and the amount of fresh charge that was expelled directly through the exhaust port during this scavenging process. Overall, the engine was found to produce low NO_x emissions and to provide almost constant volume combustion. The rapid combustion, which resulted in the simulations, could be partly attributed to the nature of the single-zone model used.

Fiveland and Assanis [88] constructed a zero-dimensional numerical model for the simulation of the complete engine cycle using methane or hydrogen as a fuel. The hydrogen combustion chemistry scheme included 11 species and 25 chemical reactions, and was modeled using the CHEMKIN libraries [70] adapted for a variable volume plenum. Heat transfer was calculated using a subset of the k–ε model under the isotropic turbulence assumption. This method yielded the characteristic velocity that was used to calculate the heat transfer coefficient.

Simulation results for a hydrogen-fueled four-stroke engine with a compression ratio of 15 and 1.5 bar intake pressure required 425 K intake charge temperature to produce ignition near TDC. This high intake temperature requirement, at a moderate compression ratio and at a low fuel–air equivalence ratio of 0.3, was necessary since hydrogen ignition occurred at about 1050–1100 K in the simulation. Under these conditions the researchers identified peaks in H, OH and HO_2 fractions near the ignition point. The simulation model was also used in a parametric investigation, in which it was found that decreasing the initial temperature or the fuel–air equivalence ratio, beyond a certain point, retarded ignition and eventually led to misfire.

3.2. Alcohols

Ng and Thomson [92] constructed a single-zone model to simulate ethanol HCCI combustion and especially the effect of ethanol reformed gas on the ignition requirement and NO_x emissions. They incorporated Marinov's set of chemical reactions [60] to simulate ethanol oxidation and integrated a NO_x reaction mechanism from GRI-Mech [84] to simulate NO_x formation. For the estimation of heat losses they used a convective heat transfer correlation (similar to Newton's Law of cooling).

The researchers conducted a parametric study, in which the parameters varied were the fuel–air equivalence ratio, the EGR amount and the degree of reforming, i.e. the degree of ethanol conversion into CO and H_2. Thus, the initial charge contained ethanol,

CO, H_2 and EGR at various proportions. It was found that fuel reforming resulted in an expansion of the HCCI operating region, the boundaries of which were determined by misfire and unacceptable NO_x emissions. However, reforming tended to increase NO_x emissions due to the resulting high peak combustion temperature. In relation to reformed gas, EGR was more effective toward expanding the simulated operating range at moderate equivalence ratios (0.2–0.5).

Martinez-Frias et al. [93] investigated the direct use of wet ethanol using a simulation model. The use of wet ethanol as a fuel reduces the energy demands for its production, since the distillation and/or dehydration processes, which are used to remove the water and provide neat ethanol, require a significant amount of energy (37% of the total energy in ethanol products for corn-based ethanol production). The objective of the study was to determine whether benefits could be obtained by the direct utilization of wet (as opposed to neat) ethanol into a turbocharged HCCI engine. The researchers constructed a simulation model for a TC HCCI engine fueled with wet ethanol (35 vol.% EtOH in H_2O). Apart from the TC, the full engine system model also incorporated an exhaust gas regenerator, a fuel vaporizer and a catalytic converter.

The HCCI engine was modeled via a single-zone model, using CHEMKIN [94] to solve for chemical kinetics. The ethanol reaction mechanism was that of Marinov [60] and the NO_x-related reactions were taken from GRI-Mech [84]. Heat transfer was also incorporated into the reciprocating engine model assuming a wall temperature of 430 K. Using this model, the researchers found that a minimum ethanol-in-water fraction of 35 vol.% (liq.) was necessary for a sustainable simulated HCCI operation. This provided an overall brake efficiency of 38.7% for the entire simulation system. The researchers estimated that this direct use of 35% wet ethanol significantly reduced the energy required for fuel production – relative to neat ethanol production – by eliminating the need for dehydration and limiting the distillation needs to 3% of the total energy in ethanol products, in the case of corn-based ethanol production.

In Ref. [95] Szybist used CHEMKIN-PRO [94] to simulate the HCCI combustion of n-heptane, isooctane, toluene and ethanol. The simulation model was switched to the adiabatic mode. The mechanism used for the simulation of ethanol combustion was that of Marinov [60] including 56 species and 351 reactions. The author used this model to simulate HCCI combustion with the aforementioned fuels under normal naturally aspirated conditions with air dilution and under negative valve overlap (NVO) conditions. In the latter case, the mixture had a higher temperature at BDC (>500 K) and a significant amount of diluents such as O_2, CO_2, H_2O and N_2. These conditions resemble HCCI under NVO operation, in which a portion of the exhaust gases is trapped within the combustion chamber and raises the temperature of the incoming fuel–air charge. The results of the study showed that with low intake temperature (325 K) and no EGR, the most resistant fuel to ignite was ethanol requiring the highest compression ratio. However, under NVO conditions toluene was the most difficult to ignite. Moreover, with NVO the ignition timing between fuels converged to within a few CA degrees, with the exception of n-heptane at high O_2 dilution. On the contrary, ethanol was essentially insensitive to the O_2 dilution, under the conditions of the simulation, indicating a zero-order reaction rate with respect to O_2. The researcher concluded that ignition in HCCI combustion under NVO conditions presented distinct features, which were not entirely consistent with the RON and MON parameters.

Yang et al. [96] also investigated NVO HCCI combustion. They used a single-zone adiabatic model to simulate the reactions taking place within the combustion chamber with the injection of gasoline, ethanol or methanol during the NVO period. The reaction kinetics was incorporated via the mechanisms of Marinov [60] for ethanol, and Lindstedt and Meyer [77] for methanol. The researchers studied both the thermal and the chemical effect of the fuel injection during the NVO period. They found that during this period both heat and active species such as H_2 and CO can be produced, depending on the fuel type, oxygen availability and the in-cylinder temperature of the residuals during injection. At relatively high oxygen availability in the residuals the tendency was to produce more heat than active species, since the fuel was oxidized. In oxygen-poor residuals only part of the fuel was oxidized producing active species. Methanol and ethanol were less sensitive than gasoline to O_2 availability owing to their oxygenated nature. Methanol showed the greatest tendency in forming active species.

3.3. Ethers

In [48] Yao et al. used the SENKIN code of the CHEMKIN package to simulate DME combustion. The single-zone model used was considered adiabatic and the chemical mechanism, which was used to describe the DME oxidation, was that of Lawrence Livermore National Laboratory including 79 species and 336 reactions [52–55]. The scope of the study was to analyze the reaction pathways of DME oxidation. The researchers validated the simulation results against experimental data, which indicated that the combustion rate and the peak combustion pressure were overestimated due to the nature of the single-zone model. However, the ignition timing was adequately predicted, implying a sufficient description of the reaction pathways. It was found that DME presented a two stage auto-ignition with low temperature reactions (LTR) followed by high temperature reactions (HTR). HCHO and OH were the primary radicals during LTR. DME ignition was controlled by the H_2O_2 decomposition to two OH radicals, which provided a chain branching step. These hydroxyls were the primary attackers for the H atom abstraction from DME and the oxidation of CO. At relatively leaner DME concentration the LTR was not significantly affected but the CO oxidation deteriorated, indicating a temperature sensitivity of the CO oxidation process. This led to the generally accepted conclusion that CO emissions in HCCI engines originate from the relatively cold and/or lean regions of the combustion chamber, such as the crevices and the vicinity of the wall, in which the local temperature is adequately high to induce partial oxidation of the existing HC but not high enough to consume the resulting CO.

Hofmann and Abraham [97] also used the internal combustion engine model included in the CHEMKIN package [94] to simulate n-heptane, DME and methyl decanoate HCCI combustion. The latter was studied as a biodiesel surrogate. The simulation model incorporated Woschni's correlation [91] for the estimation of heat losses from the combustion chamber. The primary objective of the study was the investigation of ignition delay and NO formation for the three fuels. For this purpose, the researchers used Herbinet et al. [81] detailed chemical kinetic mechanism for methyl decanoate – a biodiesel surrogate – consisting of 3036 species and 8555 reactions, and Livermore National Laboratory scheme for DME oxidation including 79 species and 351 reactions [53–55]. NO formation was simulated using two alternative schemes; the extended reaction mechanism of Zeldovich [83] and the NO kinetics from GRI-Mech v.3 mechanism [84]. The Zeldovich NO formation scheme provided reduced NO concentration relative to the more extensive NO scheme of GRI-Mech for all fuels. Moreover, it was demonstrated that DME showed the shortest ignition delay followed by methyl decanoate and n-heptane. Thus, DME required higher engine speed and the lowest initial temperature. Although the primary consideration for NO formation was the peak combustion temperature, fuel chemistry was also found to play a secondary role.

3.4. Biodiesel

Apart from Hofmann and Abraham mentioned in the preceding sub-section, biodiesel HCCI combustion was also simulated by Brakora and Reitz [98] using the SENKIN code of the CHEMKIN package [94]. The single-zone model was considered adiabatic for the purpose of the study, which was to investigate the formation of NO_x from biodiesel- and diesel-fueled HCCI engines. N-heptane was used as the diesel surrogate, and a mixture of 2/3 n-heptane and 1/3 methyl butanoate was used to simulate biodiesel combustion. This proportion of n-heptane and methyl butanoate in the biodiesel surrogate was found to yield a better approximation for the actual C:H:O ratio found in the real biodiesel, relative to neat methyl butanoate or methyl decanoate. The latter two, being relatively short chain esters, provided a much higher C:O ratio than the actual biodiesel fuel. The chemical mechanism used for the biodiesel surrogate consisted of 56 species and 169 reactions [78]. NO_x formation was incorporated via a 7 species and 19 reactions scheme, which was developed by Yoshikawa and Reitz [87] relying on reactions from the GRI-Mech mechanism [84].

Brakora and Reitz found that the ignition timing played a crucial role in the resulting NO_x emissions. With an equivalent energy release and for the same ignition timing, the two surrogates provided roughly the same peak combustion temperatures (within approximately 20 K) and yielded similar NO_x emissions at EVO. There was a difficulty in connecting the oxygen content of the fuel to the produced NO_x emissions, especially at lean mixtures. Under stoichiometric conditions, the biodiesel surrogate yielded a 26% increase in NO_x relative to the diesel surrogate. However, the predicted difference in peak combustion temperature was about 13 K lower for biodiesel, suggesting that the fuel–bound oxygen could play a role in the formation of NO_x under limited O_2 concentrations. It was also found that under the same energy content, ignition timing and total N:O ratio in the mixture, for the two fuels, the diesel surrogate yielded higher NO_x emissions. This suggested that having the same amount of O_2 available in the air, as opposed to being fuel–bound, increased the NO_x emissions due to the alteration of the heat capacity of the mixture, which resulted in higher flame temperatures for the diesel surrogate. The study concluded that under HCCI conditions, in which near stoichiometric local conditions are not encountered, any NO_x increase due to biodiesel would be small.

3.5. Fuel blends and additives

Apart from neat fuels, single-zone models have been used with fuels blends, to assess the effects of additives/blends on the HCCI combustion process.

Szybist et al. [38] used a single-zone model to simulate the combustion of biodiesel blends in HCCI engines. In their study they used CHEMKIN [94] for the chemical kinetics simulation coupled with chemical mechanisms for n-heptane [99], which represented diesel fuel, and methyl butanoate [80], which accounted for biodiesel. The combined mechanism consisted of 670 species and over 3000 reactions, including NO_x formation reactions, which were taken from GRI-Mech [84]. With this mechanism it was possible to study different blends of n-heptane and methyl butanoate, which were used as surrogates for the simulation of diesel/biodiesel blends. Thus, the researchers simulated diesel/biodiesel blends of 0, 10 and 50% (vol.) in biodiesel with n-heptane/methyl butanoate blends, the relative proportion of which was chosen to match the oxygen content (wt%) of the experimental fuel blends.

The simulation model predicted the effect of inlet temperature increase on the phasing and magnitude of the low temperature heat release (LTHR), and the phasing of the main combustion event. However, discrepancies were observed between experiments and simulation as regards the dependence of the results on the biodiesel concentration, and the duration and phasing of the LTHR and the main combustion event. These were attributed to the low cetane number of methyl butanoate, the approximation of the IVC temperature with the intake manifold temperature, and the inherent inability of the single-zone model to capture any fuel or temperature stratification. The latter resulted to an overestimation of the peak combustion temperature and the combustion rate, which led to almost 100% combustion efficiency, very low CO and high NO_x emissions.

Saisirirat et al. [100] examined the effect of n-heptane blends with ethanol and 1-butanol, both experimentally and numerically. They used the SENKIN single-zone model of the CHEMKIN II code [94] to simulate n-heptane/ethanol and n-heptane/1-butanol fuel blends. The chemical mechanism used was that of Saisirirat et al. [44] consisting of 1046 species and 4398 reactions, which includes ethanol, 1-butanol and PRF oxidation sub-schemes. The simulation compared the HCCI combustion of neat n-heptane to the one obtained with the two fuel blends, i.e. n-heptane/ethanol and n-heptane/1-butanol both in 63:37 molar proportions. It was found that the addition of ethanol or 1-butanol to n-heptane affected the OH radical production and slowed down the chemical reactions during LTHR, decreasing the concentration of reactive intermediate species (HCHO, OH, HO_2, etc.). Thus, alcohols induced a chemical effect on the LTHR. Owing to this reduction in chemically active species and to the low LTHR, which prevented a further temperature rise of the mixture, the main combustion event was delayed with the addition of alcohols.

Mack et al. [101] constructed a single-zone model for the simulation of ethanol/diethyl ether (DEE) blends. The single-zone model incorporated Woschni's correlation for the estimation of heat losses; it used a DME-derived chemical mechanism [52] for the chemistry of DEE oxidation, and Marinov's ethanol oxidation scheme [60] for the combustion chemistry of ethanol. The combined mechanism consisted of 112 species and 484 reactions. The purpose of the study was to investigate the relative reactivity of DEE and ethanol in a fuel blend of 25% DEE in ethanol. The experiments conducted with carbon-14 isotope tracing showed that DEE was more reactive than ethanol, yielding more CO_2 relative to ethanol. The simulation results supported this conclusion, since it was found that DEE began to react earlier than ethanol. However, a significant elongation of the heat release, which would be desirable to control the combustion process, was not observed using the fuel blend.

The same research group also studied the effect of small amounts of di-tertiary butyl peroxide (DTBP) (up to 3%) on the HCCI combustion of ethanol and diethyl ether blends [45]. The intention was to elongate the combustion event using the exothermic decomposition of DTBP to promote early DEE ignition. The single-zone model used was the one mentioned earlier and the combustion reaction scheme was enhanced by the adiabatic decomposition of DTBP based on the work of Iizuka et al. [102]. It was found via simulation, and verified by experiments, that the addition of DTBP advanced the ignition timing in the DEE-ethanol blend. The simulations showed that the decomposition of DTBP raised the temperature of the mixture and advanced ignition, although potential chemical effects of DTBP were not excluded.

Yao et al. [103] used a zero-dimensional thermodynamic model coupled with CHEMKIN III to simulate a DME/methanol blend in an HCCI engine. The chemical mechanisms used were the ones of Curran et al. for DME [52], consisting of 78 species and 336 reactions, and Held and Dryer [74] for the reactions of methanol, consisting of 22 species and 89 reactions. The authors compared the simulation predictions to experimental results of pressure and operating range in $\lambda_{DME} - \lambda_{MeOH}$ map. The analysis of the simulation results showed that in DME/methanol dual fuel oxidation the low temperature heat

release of DME was inhibited, resulting only in a high temperature heat release. The OH radicals were mainly formed by the decomposition of H_2O_2 at blue-flame reactions, and by $H + O_2 = O + OH$ and $O + H_2O = OH + OH$ at hot flame reactions.

Similar results were found by the same Institute in another study [104]. The simulation model used has already been described in the first part of their paper [48] presented in Section 3.3. In Ref. [104] the researchers studied the HCCI combustion of a DME/methane blend. Under the simulation conditions, the dual fuel blend showed a two stage autoignition scheme. This was different from the classical two stage ignition observed in neat DME oxidation, since it corresponded to two high temperature heat release rates, one of DME, which was found to oxidate first, and the other of methane. It was observed that methane - like methanol - inhibited the LTHR but promoted the high temperature heat release (HTHR) of DME. On the other hand, DME promoted methane oxidation both due to thermal and chemical considerations. The thermal effect was due to the temperature increase, which was the result of DME oxidation, while the chemical effect was due to HCHO and H_2O_2, which were formed during DME oxidation and increased the OH radical pool. The researchers also identified the major reaction paths for the dual-fuel oxidation.

In [105] Ogawa et al. studied the suppression effects of additives such as water, methanol, ethanol, hydrogen and methane, on the combustion of a DME fueled HCCI engine. The researchers used SENKIN under adiabatic conditions for the single-zone simulations and the corresponding chemical mechanisms were adapted from Curran et al. [52] for DME, Marinov [60] for Ethanol, and Westbrook et al. [75,76] for Methanol. In the experiments the suppressors were injected directly into the combustion chamber, while the DME was introduced into the air stream at the intake pipe. The direct injection of suppressors induced a cooling effect on the charge. Water injection had a predominantly cooling effect, i.e. it lowered the temperature of the mixture during its vaporization, thereby retarding ignition. Simulations conducted with the assumption that gaseous water was introduced in the mixture at BDC, resulted in a slight delay in radical formation and suggested that the water addition also had a minor chemical effect. Similar findings characterized methanol addition. Its main effects were a thermal one observed during the experiments and a chemical one suggested by simulations.

As in the case of water addition simulations, methanol addition simulations were conducted assuming that methanol existed in gaseous state at the beginning of calculations. It was found that methanol addition severely suppressed LTHR to near-zero values, significantly reduced OH, H and O radicals, and retarded main combustion. Further simulations with ethanol, hydrogen and methane addition showed that LTHR was slightly reduced with hydrogen or methane addition, and essentially disappeared with the addition of ethanol or methanol, in order of significance. Moreover, it was found that despite the different simulation conditions with respect to additive and its quantity, the OH concentration at the onset of LTHR remained fairly constant. This suggested that the chemical effect induced by the additives was linked to a reduction in the OH radicals prior to LTHR.

This assumption regarding OH radicals was supported by later studies with H_2 and MeOH addition to DME–air mixture. Specifically, Shudo et al. [106,107] investigated the effect of H_2 addition, which originated from on-board methanol reformed gas, on the DME HCCI combustion. The concept of the combustion engine system and the experimental setup are given in Fig. 6(a) and (b).

The SENKIN [94] simulation model was used to describe the effect of hydrogen addition, and the reaction mechanism used was that of Fischer et al. [53–55] consisting of 79 species and 351 reactions. The simulation results showed that the addition of H_2 in the DME–air mixture suppressed DME consumption. This was due to an

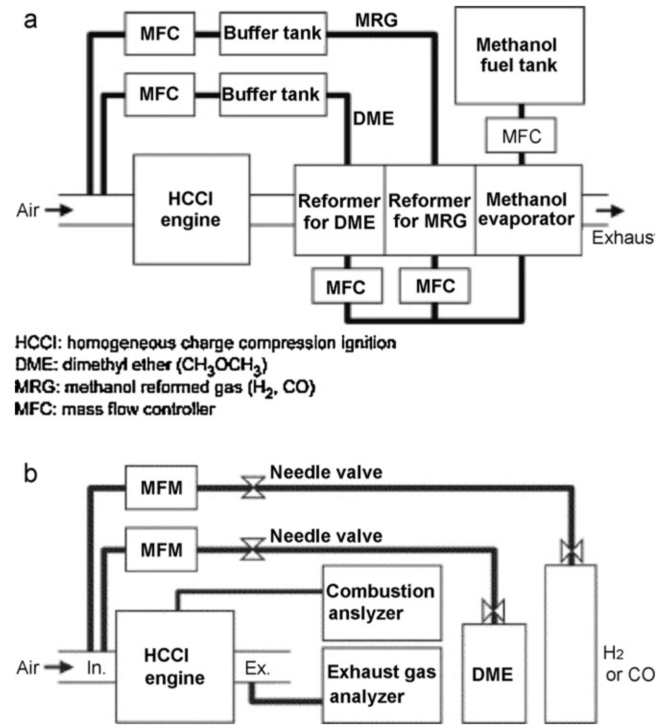


Fig. 6. (a) Concept of HCCI combustion engine system fueled with DME and MRG onboard-reformed from methanol utilizing engine exhaust gas heat [107] and (b) experimental setup [106].

antagonistic effect for the consumption of OH radicals; in the presence of H_2, OH radicals reacted preferentially with H_2 instead of DME, to yield the relatively stable – at low temperatures – intermediates HO_2 and H_2O_2. This led to a suppression of LTHR, a decrease in the in-cylinder temperature rise and a consequent retardation of the main combustion event. This thermal effect was the main reason for the combustion retardation, since the ignition temperature was not altered appreciably. These findings implied that hydrogen or hydrogen-containing additives, such as methanol reformed gas (MRG), could be used to control the ignition timing of DME. The researchers also studied the conversion of methanol to DME and H_2, via dehydration- and thermal decomposition-methanol reformers, respectively, to conclude that the H_2/DME fraction in MRG could be continuously controlled by adjusting the methanol supply in each reformer. The addition of CO in neat DME, which was studied in [106], was also found to suppress the DME oxidation at low temperature, but its effect was less pronounced than the H_2 addition effect.

Yamada et al. [108] studied the effect of methanol or O_3 addition to DME-air mixture under HCCI combustion conditions. They used the SENKIN [94] code to simulate the engine operation, and implemented a chemical mechanism by Curran et al. [52] to account for the DME and methanol addition chemistry. Ozone addition was accounted for by including the thermal decomposition reaction of ozone according to Heirmel and Coffee [109]. The experimental and simulation results showed that methanol addition retarded the main heat release event significantly; 8% addition of methanol in DME resulted in a 15° CA delay. It was suggested that this delay was due to the competitive consumption of OH by methanol instead of DME, which led to the formation of relatively stable intermediates such as HCHO and HO_2. In contrast, the addition of low O_3 amounts (0.015% in DME) advanced the ignition timing by as much as 20° CA. This was due to the decomposition of O_3 at relatively low temperatures (~600 K), which provided oxygen atoms and activated the mixture. This supply of oxygen atoms at temperatures lower than

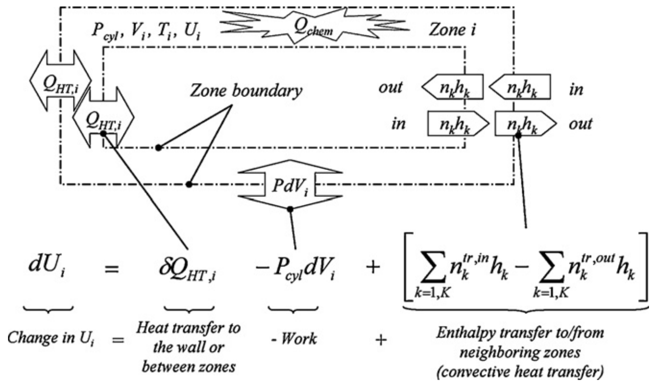


Fig. 7. The First Law of Thermodynamics applied to a zone of a multi-zone model.

those of normal cool flames suppressed the production of formaldehyde, which was a chain termination step under low temperatures. Thus, more heat was liberated during cool flame reactions, leading to an earlier thermal ignition.

4. Multi-zone modeling

The limitations encountered with single-zone models can be partly overcome with the use of multi-zone models. The latter assume that the combustion chamber is divided into a sufficient number of regions or zones, each possessing uniform thermodynamic properties. The sufficiency of the number of zones is usually determined by a sensitivity analysis, i.e. the minimum number of zones used is defined as the number beyond which the simulation results tend to converge.

The temperature, composition, volume and all thermodynamic properties of each zone are considered uniform within the boundaries of the zone, but can be different from the thermodynamic properties of other zones. This provides an opportunity to study the effects of temperature or species stratification within the combustion chamber, and usually leads to a better estimation of the combustion duration, the pressure rise rate and the emissions formation. Mass and heat transfer within the combustion chamber play a critical role in the estimation of the aforementioned operating characteristics and since the combustion chamber is considered an ensemble of thermodynamically distinct zones, the processes of mass and heat transfer between zones must also be described by the multi-zone model. Fig. 7 shows the first law of thermodynamics applied to a zone, which in the general case includes heat and mass transfer. As regards mass transfer, each zone can be thermodynamically defined as a closed or an open thermodynamic system, depending on whether mass flow between zones is prohibited or allowed, respectively. Likewise, heat transfer between zones and to the combustion chamber wall can also be permitted or neglected.

However, the assumptions regarding mass and heat transfer affect the results of the simulation significantly; heat transfer affects the temperature stratification within the combustion chamber, the colder regions of which are sources of unburned HC and CO. The formation of these pollutants is also affected by mass transfer between zones, since any HC or CO flowing from a colder to a hotter region/zone is expected to be (partially) oxidized [110]. The predicted combustion rate, pressure rise rate, combustion duration and peak pressure are also affected by the choice of the submodels used to describe heat and mass transfer. The multi-zone models examined subsequently are divided into stochastic based multi-zone models, in which some properties of the mixture are considered random variables, and phenomenological multi-zone models, in which probability considerations have been excluded.

In [62] Mosbach et al. constructed a stochastic reactor model (SRM) based on a probability density function (PDF) approach. The PDF was approximated by an ensemble of 100 stochastic particles. These did not contain any spatial or geometric information. The random variables were the species concentration and the temperature. The model included heat transfer to the combustion chamber wall using Woschni's correlation [91] and the magnitude of the temperature fluctuations was regulated by a coefficient. Turbulent mixing was accounted for via a mixing intensity term that included the characteristic mixing time. The fuel simulated was a blend of EtOH/DEE, although a validation of the model was also presented with neat EtOH as fuel. The validation showed good agreement between experimental and simulated results as regards pressure traces. The model also captured qualitatively the experimental variation of CO and HC emissions with the combustion phasing, i.e. the angle at which 50% of the total heat has been released. In these simulations, the equivalence ratio remained constant and the combustion phasing was regulated via the initial temperature. The stochastic reactor model was also used to study numerically the effect of the DEE in EtOH ratio on the combustion phasing, the combustion duration and the emissions of the HCCI engine. It was shown that as the fraction of DEE in the DEE/EtOH blend was increased, the combustion phasing advanced before TDC, the combustion duration was shorter, and the CO emissions were reduced. This fact provided indication that DEE could be used with ethanol to regulate the combustion phasing and duration of the HCCI combustion.

Noda and Foster [111] numerically studied hydrogen HCCI combustion by constructing a multi-zone model; the different zones catered for any temperature or composition inhomogeneities. The zones were not assigned a specific location within the combustion chamber, and mass exchange between them was neglected. The heat losses were calculated via the Woschni [91] correlation using the combustion chamber area and the mean gas temperature. The combustion chemistry was accounted for by incorporating 11 species and 23 reactions from Westbrook and Dryer [69] for the oxidation of hydrogen, and the extended Zeldovich mechanism of Lavoie et al. [83] for NO_x formation. The researchers used 10–30 zones to examine the effect of temperature and fuel inhomogeneities on HCCI combustion. Both temperature and – to a much lesser degree – fuel inhomogeneities increased the combustion duration compared to single-zone simulations. The mean gas temperature and the type of temperature inhomogeneity also affected combustion duration and the formation of NO emissions. Provided the mean gas temperature was high enough to avoid bulk quenching of the mixture, the most favorable type of temperature stratification included a small amount of hot gases to induce autoignition and avoid excessive NO formation and a greater amount of colder mixture. This type of stratification expanded the operating range in a mean gas temperature versus temperature inhomogeneity map.

Komninos et al. [112] and Komninos and Rakopoulos [40,113] used a multi-zone model to simulate hydrogen [112] and ethanol [40,113] HCCI combustion. In all studies, the multi-zone model used divided the combustion chamber into several zones, which occupied specific geometric regions (Fig. 8).

The only uniformity assumed was that of pressure, while heat and mass transfer between zones was accounted for, taking into account the geometric configuration of the zones; each zone could communicate with its immediate inner and outer zone (Fig. 9). The model also accounted for a crevice zone, which was in direct communication with the outmost zone of the combustion chamber. In Ref. [112], 11 zones were used – including the crevices – to simulate hydrogen HCCI combustion and the Annand correlation [114] was employed to estimate the heat flux from the outmost zone to the combustion chamber wall. The chemistry of hydrogen oxidation

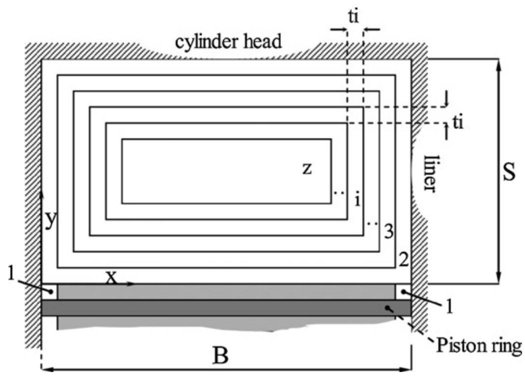


Fig. 8. Zone configuration in the multi-zone model [112].

was accounted for via the mechanism of Marinov et al. [54] involving 10 species and 19 reactions, augmented by a NO_x formation scheme adapted from the isooctane oxidation reaction mechanism of Golovitchev [86]. A parametric investigation was conducted with the multi-zone model to determine the effect of various operating parameters on hydrogen HCCI combustion. Compression ratio and initial temperature were the dominant factors affecting the ignition timing and pressure rise rate. Engine speed also affected the ignition timing, mainly due to the variation of the available time for the occurrence of chemical reactions. It was found that increasing the load, i.e. the equivalence ratio, NO_x emissions were increased significantly. Inlet pressure increased almost proportional to the attainable imep, without compromising the fuel conversion efficiency for the conditions simulated.

In [40] Komninos and Rakopoulos numerically compared ethanol and isooctane HCCI combustion. The multi-zone model used was the one described in the preceding paragraph with some modifications; the zones number was increased to 16, the zone resolution was refined near the combustion chamber wall, and the wall heat flux estimation approach abandoned the Annand correlation and was based on the temperature gradient near the wall. These modifications were necessary to better estimate the formation of HC and CO emissions [115]. The chemical mechanism used for the ethanol oxidation was that of Röhl and Peters [57] consisting of 38 species and 228 reactions. Since this mechanism did not include NO_x reactions, it was augmented by 13 reactions involving nitrogen oxides formations [86]. The model vas validated against

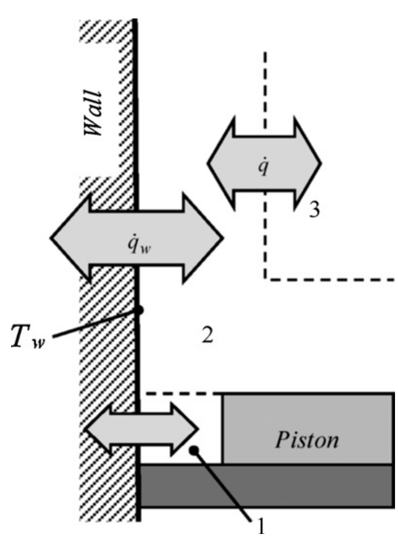


Fig. 9. Schematic of heat transfer between zones and to the cylinder wall [113].

experimental results and captured adequately the pressure traces and HRR for both ethanol and isooctane.

According to the simulation results, CO emissions were formed near the combustion chamber walls, thereby justifying the finer zonal resolution used in these regions (see Fig. 10). As shown in Fig. 10, the amount and location of CO production was found to depend on load; at higher loads, CO production advanced to the inner zones.

Total CO emissions were adequately captured but HC emissions were overestimated, especially for ethanol. An investigation for the composition of the HC emissions for both isooctane- and ethanol-fueled HCCI combustion showed that in the ethanol cases examined the vast majority of unburned HC consisted of oxygenated HC species (OHC). These were primarily ethanol, acetaldehyde and formaldehyde. The predicted percentage of OHC in total HC (aprox. 95% by mass) for ethanol was not very sensitive to the load variation under the simulation conditions. On the contrary, the relative amount of OHC in total HC was lower (19–33% by mass) in the case of isooctane and decreased with the increase of load. It was concluded and demonstrated that this would induce a significant error in the HC measurement if a measuring device such as the FID was used, since the FID principle possesses an inherent inability to accurately detect oxygenated carbon atoms [116].

Using the same model in [113] the authors compared two ethanol oxidation mechanisms, namely Marinov's [60] and Röhl and Peters' [57]. Marinov's mechanism consisted of 57 species and 383 reactions, while Röhl and Peters' mechanism, which was a reduced version of Marinov's, consisted of 38 species and 228 reactions. Both mechanisms were augmented by NO_x related reactions taken from [86]. The results showed that the two mechanisms predicted essentially the same dominant HC species, with the exception of formic acid (HCOOH) and to a lesser extent methanol (CH_3OH), both of which were not included in the reduced mechanism. The mechanism reduction had a significant impact on the computational time: although the species used in Röhl and Peters' mechanism were 2/3 of the species used in the Marinov mechanism, the Röhl and Peters' mechanism required half the computational time. The simulation results showed a slightly higher predicted combustion rate by the Röhl and Peters' mechanism relative to Marinov's mechanism, despite the fact that the predicted initial heat release was the same for the two mechanisms. The resulting temperature fields were almost identical as shown in Fig. 11. Therefore, the two chemical mechanisms did not induce significant differences in the predicted performance. NO_x, CO and HC emissions were essentially the same for the two mechanisms, with the greatest disagreement occurring between predicted CO emissions (~9%) at the low load cases. This was connected with the slightly lower combustion rate predicted by Marinov.

Sjoberg and Dec [117,118] used a multi-zone model to study the effects of engine speed, equivalence ratio, initial temperature and boost pressure on ethanol HCCI combustion. They used the multi-zone model provided by the Senkin application of the CHEMKIN package [94], which treated each zone as a single lumped mass with uniform composition. The only interaction between zones was through pressure, which was considered uniform. Thus, the volume of each zone depended on its mass and its temperature relative to the other zones. The 11 zones used were adiabatic in principle. This led to the need to introduce initial temperature stratification for the 10 active zones to match the experimental pressure trace. The 11th zone was assigned a temperature low enough to render it chemically inactive throughout the engine cycle. This zone included 16% of the total mass and compensated for the combustion inefficiencies, heat transfer and blow-by, which were not directly modeled. The simulated compression ratio was also reduced relative to the experimental one to account for the

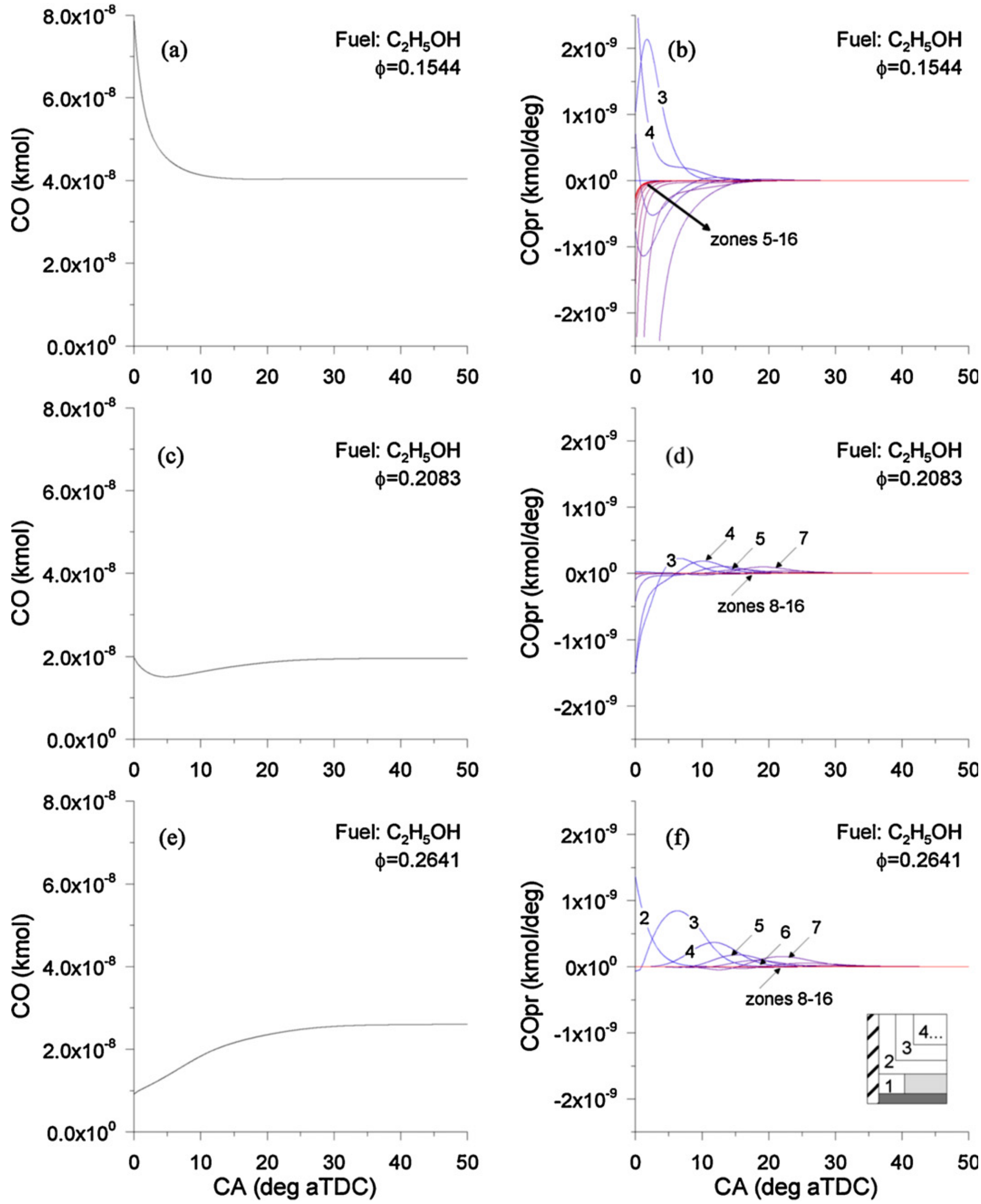


Fig. 10. CO simulation results for ethanol; left: in-cylinder CO emissions and right: zone CO production rate [40].

neglected heat losses. The thermal stratification of the zones was supported by KIVA simulations and reproduced adequately the variation of combustion phasing with temperature. The chemical mechanism used consisted of 58 species and 310 reactions [61], and was part of a larger gasoline surrogate mechanism produced by the joint effort of the National University of Ireland–Galway and Lawrence Livermore National Laboratories [119].

The simulations above showed that the ethanol oxidation mechanism reproduced adequately the effect of equivalence ratio, engine speed and boost pressure on ignition. The same model was used by these researchers to study the effect of EGR and its constituents on the HCCI autoignition of ethanol [118]. In this study, it was found that the addition of simulated EGR did not affect significantly the ethanol autoignition timing for the conditions examined. The effect of EGR on other fuels, such as isooctane and PRF, was more pronounced. This was mainly owed to the low sensitivity of ethanol oxidation on oxygen concentration, which was reduced with the increase of simulated EGR. Moreover, it was suggested that the presence of water in the EGR promoted ethanol auto-ignition.

5. Multi-dimensional modeling

Besides the aforementioned favorable attributes of the multi-zone models, they also have limitations. Even in the cases where spatial considerations have been accounted for by multi-zone models, they usually do not allow high local resolution. Moreover, there is an inherent difficulty to fundamentally describe the motion of the charge within the combustion chamber and the effects of turbulence. The problem is even more pronounced in the case of Diesel-like HCCI engines, in which the mixture formation is achieved via direct fuel injection within the combustion chamber. Direct fuel injection imposes new demands on any simulation model, since the mixture – and the resulting temperature – stratification within the combustion chamber is affected significantly by

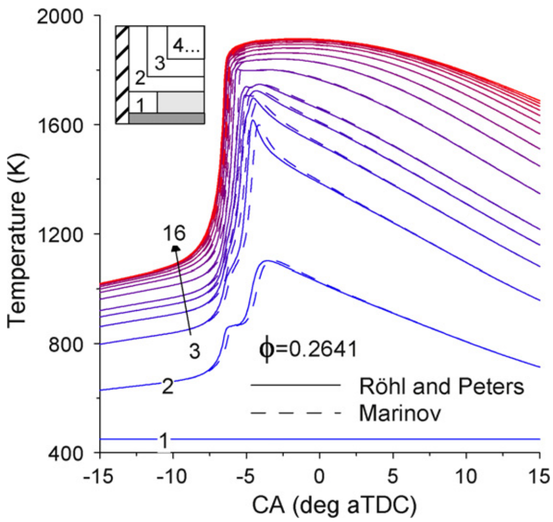


Fig. 11. Zone temperature distributions produced by Röhl and Peters' (solid line) and Marinov's (dashed line) mechanisms for the high load ethanol case ($\phi = 0.2641$) [113].

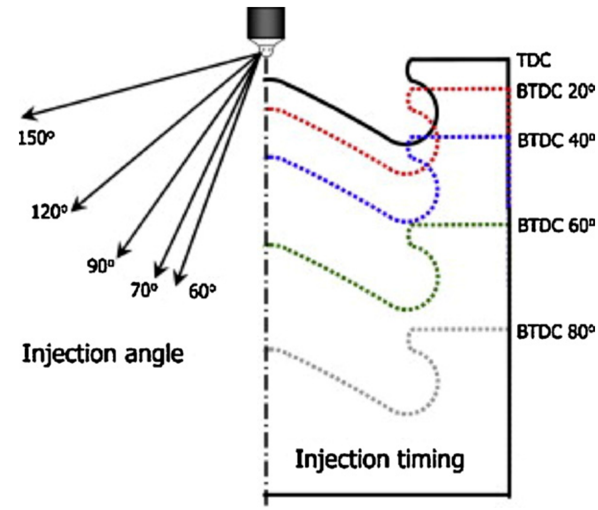


Fig. 12. Cylinder locations according to the injection timing and five injection angles [120].

the injection characteristics. Phenomena such as wall wetting, fuel dispersion, fuel vaporization under the low pressure-low temperature conditions encountered during early direct injection, must be described. In these cases, the incorporation of accurate models for the estimation of the physicochemical fuel properties becomes crucial, especially for biofuels, since their development and use has a relatively short history.

The aforementioned issues can be dealt with by using multi-dimensional models, i.e. CFD models, which describe in detail the charge motion within the combustion chamber and the turbulence effects, provide a superior spatial resolution of the combustion chamber, and can account for the description of DI HCCI combustion by incorporating the dynamics and kinematics of the fuel injection.

In the remaining part of this section, direct injection HCCI CFD models will be discussed first while dedicated HCCI CFD models assuming homogeneous conditions at IVC will be presented subsequently.

5.1. Direct injection HCCI

Kim et al. [120] investigated the influence of the spray angle and advanced injection timing on the combustion performance and emission characteristics in a DME fueled compression ignition engine. They used the KIVA software [121], which was supplemented with liquefied DME fuel properties and their temperature dependence [122–126]. The oxidation process of the DME fuel was described with a detailed chemical kinetic model [53–55], which consisted of 351 reversible elementary reactions among 79 species. This mechanism was expanded by including NO_x formation reactions taken from a modified version of GRI Mech [84]. A two-step phenomenological soot model [127] was also applied to calculate soot emissions. The DME spray and atomization characteristics were simulated via the Kelvin–Helmholtz (KH) and Rayleigh–Taylor (RT) hybrid breakup model [128]. Turbulence was accounted for via the modified Renormalization Group (RNG) k–ε model [129], and wall impingement was simulated via the spray wall interaction model [130] including droplet splash/spreading. A computational grid with a unit cell size of about 2 mm^3 was formed for the evaluation of spatial distribution in the cylinder and the computational grid was divided into a 60° sector mesh, due to the symmetric arrangement of the six-hole injector. The calculation time step was set at 0.1 μs.

The model was validated against experimental measurements at three injection timings, with an injection angle of 156°. The experimental and simulation results at an injection timing of 60° BTDC had two peaks in the heat release rate, indicating low- and high-temperature DME oxidation. The validated model was subsequently used for a numerical study aimed at analyzing the effect of the injection angles and timings shown in Fig. 12. The resulting fuel spray patterns created by these configurations are shown in Fig. 13. These patterns revealed fuel spray-wall interactions and accumulation of fuel in the squish area and, possibly, the crevice regions.

Generally, the fuel injected vaporized rapidly as it entered the combustion chamber due to the high volatility of DME. At an early injection timing (60° bTDC), the variation of the injection angle affected significantly the pressure and heat release rate diagrams; at wider injection angles the peak pressure and HRR were both reduced, since some of the injected fuel reached the relatively cold crevice and combustion chamber wall regions. At later injection timings, the effect of the injection angle was much less pronounced, since the fuel was injected within the piston bowl. As the injection timing approached TDC, the combustion mode shifted progressively from partially homogeneous to diffusive combustion. Soot emissions were very low for all cases examined due to the chemical structure of the fuel, which excludes C–C bonds. Another reason was the relatively premixed nature of the mixture, especially at early injection timings.

NO_x emissions were very low for the early injection timings (IT 40° bTDC and earlier) due to the premixed nature of the mixture. As the injection timing approached TDC, NO_x emissions increased, probably owing to the predominance of the in-cylinder inhomogeneities. At advanced injection timings and/or wide injection angles, the HC and CO emissions were higher due to the introduction of fuel into the squish and crevice regions. At narrow angles, the high HC and CO emissions were due to the fuel impingement on the piston bowl. As regards performance, a narrow angle produced low ISFC at relatively advanced injection timing. Other studies focusing solely on the spray characteristics of DME by the research group of the Hanyang University can be found in [131,132]

Chen et al. [133] investigated experimentally and numerically the effect of methanol injection timing in a DME/MeOH dual fuel engine, in which the DME was introduced at the inlet port. For the numerical simulation of the closed part of the engine operation, the researchers coupled chemical kinetics with the CFD code FIRE [134]. The chemical mechanism used to estimate the

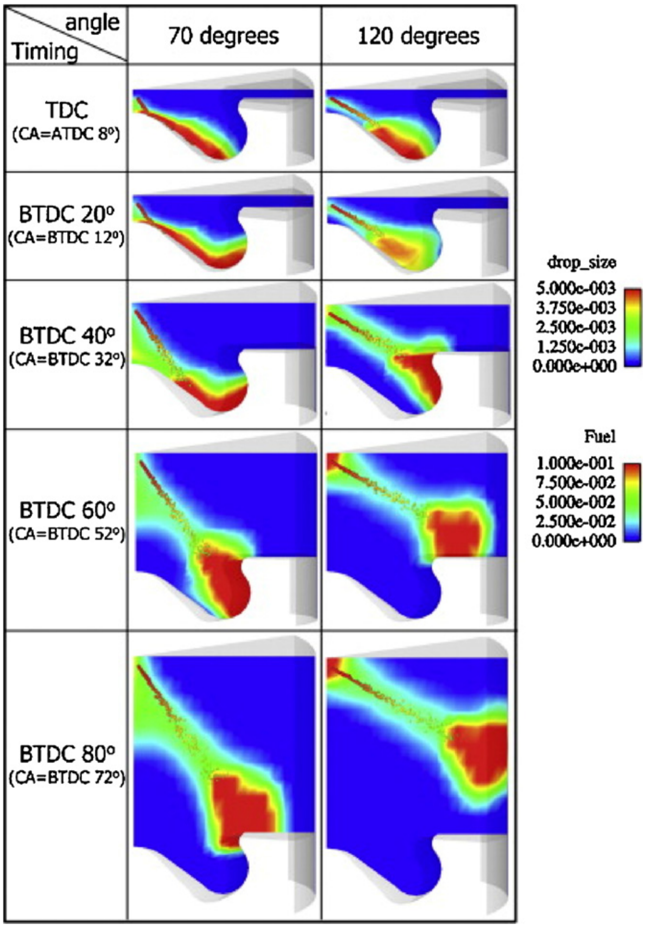


Fig. 13. Effect of the injection angle and timing on calculated spray and evaporation distributions in the cylinder according to the crank angle [120].

methanol/DME reaction rates consisted of 30 species and 44 reactions including the fuel chemistry [50], the Zeldovich mechanism, and the N_2O intermediate mechanism [82]. The effect of turbulence was accounted for by adopting a compressible version of the standard two-equation k–ε turbulence model. The source terms in the transport equations of FIRE were calculated with the assumption that the reaction rate is mainly determined by kinetic and turbulent time scales. Major submodels used in the computation included the WALLJET1 wall interaction model, the Dukowicz evaporation model, and the HuhGosman breakup model [135]. The Han-Reitz wall heat transfer model was used to estimate the wall heat flux [136]. The spray angle was 152° formed by a 7-hole injector, which allowed for the simulation of a 51° sector consisting of 30,000 grid cells at BDC. The simulations examined the effect of MeOH injection at two injection timings, namely −26° and −6° aTDC.

It was found that methanol injected at −26° aTDC had no effect on the low temperature reaction of DME but accelerated the heat release of the high temperature reaction, producing locally high temperature regions and increasing NO concentration. In this case, the injected methanol was completely oxidized. At the later injection timing (−6° aTDC) the DME found in the crevices was higher, and the high temperature region was dispersed in the clearance volume and the region near the combustion chamber wall, leading to lower NO concentration. Some methanol vapor remained in the combustion chamber prolonging the combustion duration. This led to an investigation aimed at decreasing the combustion duration at this – relatively late – injection timing. The researchers studied numerically the effect of injection pressure on the combustion duration, while maintaining the injection timing

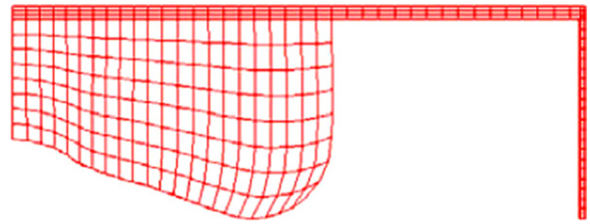


Fig. 14. Computational mesh of combustion chamber at TDC used in [138].

at −6° aTDC. They found that increasing the injection pressure from 20 to 30 MPa shortened the combustion duration, increased the thermal efficiency, and induced an increase in peak temperature and NO concentration. However, it was difficult to experimentally examine the effect of increased injection pressure due to the low viscosity of methanol.

5.2. Fully premixed HCCI

In Ref. [137] Yao et al. examined the HCCI combustion of a dual fuel engine fueled with DME/MeOH blends. They used the STAR-CD/KINETICS CFD code to simulate the combustion of the charge that was uniform at IVC. The RNG k–ε model was included to account for the effects of turbulence, and the PISO algorithm was used for the transient flow of the engine. The CFD code was coupled with the CHEMKIN code to obtain the species concentration evolution, and the DME/methanol oxidation was described by a reduced mechanism consisting of 27 species and 35 reactions [50]. The time step corresponded to 0.1° CA at an engine speed of 1400 rpm. The researchers validated the model results against an experimentally obtained pressure diagram and found adequate agreement with the measurements. Under the same experimental conditions they also conducted an investigation into the formation of HC and CO emissions. They found that UHC emissions mainly consisted of the unburned fuels and CH_2O. The unburned DME and methanol mainly resided in the piston-ring crevice region, while most of the CH_2O emissions were located next to the cylinder-liner wall. CO emissions were mainly found in the regions near the top surface of the piston.

The authors also studied the effect of load (in terms of equivalence ratio) and the relative proportion of DME in the fuel blend on the HC and CO emissions. Increasing the DME ratio, while maintaining the overall equivalence ratio, improved the combustion efficiency and reduced the HC and CO emissions. Moreover at all loads examined, a critical value for the DME ratio was found; when reducing the ratio below this value induced a significant increase in both CO and HC due to incomplete combustion. However, the critical DME ratio was not the same for all equivalence ratios examined. At high equivalence ratios, the critical DME ratio shifted toward higher values due to the increase in methanol concentration at high loads, which induced an inhibiting effect on DME ignition. A critical value was also found for the peak combustion temperature (1400 K), above which the HC and CO emissions were greatly reduced. When the load, i.e. the overall equivalence ratio, was increased while maintaining the DME proportion, HC and CO emissions were reduced.

Using roughly the same simulation model, Huang et al. [138] studied numerically the HCCI combustion of a DME fueled engine. A reduced chemical mechanism for DME HCCI combustion process was adopted, which was proposed by Yao et al. [48] and Liang et al. [49]. The reduced chemical mechanism was derived from the detailed chemical mechanism and consisted of 26 species and 28 reactions. A single layer grid was applied with an average cell size of about 2 mm, yielding about 1658 cells at IVC in the combustion chamber (Fig. 14).

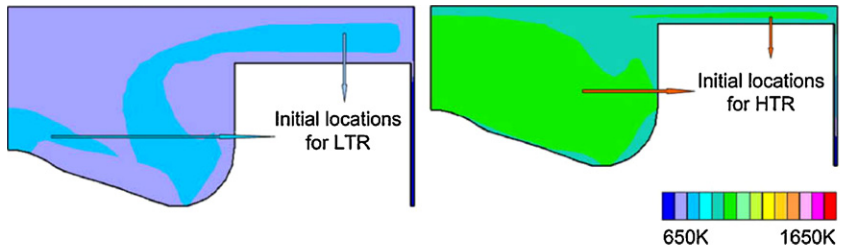


Fig. 15. Initial locations for LTR and HTR in [138].

The computational time for the closed part of the engine cycle was approximately 18 h in a Pentium IV 3.0 GHz CPU PC with 1 GB memory. Under homogeneous charge IVC conditions, the DME HCCI combustion process does not take place in the entire combustion chamber simultaneously. The low temperature reaction was initiated primarily at the region near the piston surface and the squish region, and subsequently moved toward the cylinder head. The high temperature reaction was initiated in the combustion chamber core zone and squish region, and next proceeded to the rest of the combustion chamber (Fig. 15).

The majority of HC emission was unburned fuel and CH_2O, and resided with CO in the bottom, middle, and upper part of the piston-ring crevice regions, respectively. At very low loads, DME was partially oxidized producing unburned HC and CO. As the load increased, the unburned HC decreased and the CO emissions increased and then decreased. This behavior can be explained considering the successive steps through which the hydrocarbon oxidation takes place, i.e. the oxidation follows the general scheme $HC \rightarrow CO \rightarrow CO_2$. At extremely low loads the fuel and any unburned HC produced by its decomposition fails to be converted to CO to a great extent. At higher loads, the HC to CO conversion takes place more vividly and, at the highest attainable loads, both HC and CO are oxidized to produce CO_2 through the aforementioned generalized oxidation scheme.

Chun-Ian et al. [56] simulated neat DME HCCI combustion. They used a single-zone model to compare two chemical mechanisms: a detailed mechanism of 97 species and 457 reactions, which was obtained by combining the mechanism from Curran et al. [54] with the NO_x formation reactions of Marinov [85], and a simplified reaction mechanism of 36 species and 73 reactions. The latter included a low temperature, a negative temperature coefficient, and a pyrolysis and oxidation submodel along with the reaction path for NO_x formation.

The FLUENT CFD software was also used to obtain insight into the formaldehyde and formic acid formation process during the DME HCCI combustion. For this reason the CFD code was coupled with the three submodels, i.e. the low temperature, the negative temperature coefficient, and the pyrolysis and oxidation submodels. The RNG k–ε turbulence model and the EDC combustion model were implemented in the CFD code. Using this model, the researchers found that both formaldehyde and formic acid existed in the exhaust. Their concentration was close to the experimentally determined, in the case of formaldehyde, but the measured formic acid was much less than the one predicted. The CFD calculations showed that the formation of these species was located at the region near the combustion chamber wall and above the ring crevices. Their formation originated from the partial oxidation of DME, which had entered the crevices during combustion and flowed back to the combustion chamber during expansion. The partial oxidation of DME gave rise to formaldehyde and formic acid, the further oxidation of which was suppressed due to the low local temperatures induced by the gas expansion and heat transfer to the cylinder wall. Some of the formaldehyde and formic acid formed were transferred to the central part of the combustion chamber, due to mass transfer, indicating that their concentration can be affected by the combustion chamber configuration and the existing flow field. At EVO a relatively high concentration of these gases remained near the wall.

In Ref. [139] Park numerically analyzed the combustion and emission characteristics and the optimal operating conditions of homogeneous charge compression ignition (HCCI) engines fueled with dimethyl ether (DME). For this investigation, a modified version of KIVA-3V code [121] was used to simulate DME HCCI combustion with a two-dimensional computational mesh. The CHEMKIN chemistry solver [70] was integrated into KIVA-3V, in order to solve the chemistry and the chemical mechanism used for the simulation of DME consisted of 351 reactions and 79 species [53–55]. A two-step phenomenological model was used to simulate soot emission, since the study extended the investigation into rich DME combustion. The soot model considered both soot formation, using a modified Hiroyasu model that considers acetylene (C_2H_2) as a soot precursor [140], and soot oxidation employing the Nagle–Strickland–Constable model [141]. For NO_x emissions, a mechanism derived from the Gas Research Institute (GRI) NO mechanism [84] was used.

During the simulations, the charge was assumed homogeneous at intake valve closure. The researcher generated an equivalence ratio versus peak temperature operating map based on numerical simulations, and compared the DME operation to n-heptane operation. High CO concentration was found at low peak combustion temperatures and rich mixtures. CO emissions for DME were greater than those for n-heptane, because of a lower initial mole fraction of oxygen. HC emissions for DME and n-heptane were quite similar at lean mixtures. However, HC emissions for DME were lower than those for n-heptane below a peak cycle temperature of 1600 K and an equivalence ratio higher than 1.5. Although such operating regimes are outside the usual HCCI operating conditions, this finding indicated that at low temperature-high equivalence ratio combustion conditions HC emissions can be reduced by substituting DME for diesel fuel. The optimal operating range for the best ISFC or imep is at low peak cycle temperature and below stoichiometric for both fuels, because ignition is near TDC for that area. Total heat release of DME is close to that of n-heptane in this study. The optimal operating range, which was based on a merit function including emissions and performance, was between 1700 and 1850 K peak cycle temperature and below 0.5 equivalence ratio for DME HCCI engines.

Kong [142] studied numerically and experimentally the dual fuel DME-methane oxidation in an HCCI engine. The researcher used an improved version of the CFD code KIVA-3V [121]. The CHEMKIN chemistry solver [94] was integrated into the KIVA-3V code for solving the chemistry during multi-dimensional engine simulations. A detailed reaction mechanism for DME [53–55] was used to simulate fuel chemistry, consisting of 79 species and 351 reactions. This mechanism was enriched by NO_x-related reactions obtained from a NO mechanism, which was derived from the Gas Research Institute (GRI) NO mechanism [84]. The final scheme consisted of 83 species and 360 reactions. These reactions included the

oxidation chemistry of methane, which was used to simulate natural gas. Turbulence was modeled via the RNG k–ε model and a new wall function was constructed to calculate the wall heat flux, which accounted for the variation of the gas density and the turbulent Prandtl number in the boundary layer assuming quasi-steady conditions.

Using this model, the researcher found that as DME concentration decreased ignition delayed and combustion duration was prolonged. In contrast to methane, DME experienced two-stage ignition and was depleted before any significant oxidation of methane. During the first stage of heat release, a noticeable amount of CO was formed, which was later increased during combustion and decreased rapidly only after both methane and DME were nearly consumed. The combustion of methane was induced by the high temperatures resulting from DME combustion. NO_x emissions were much lower than those in conventional diesel engines, due to the low combustion temperature. It was found that there was a minimum requirement in DME concentrations for HCCI combustion regardless of natural gas concentrations, in order to obtain stable combustion. Moreover, the operating limits – defined by misfire and knocking combustion – narrowed as the methane concentration increased, implying that high methane concentrations induce combustion instability under the conditions examined. This was probably the result of the rapid combustion of methane, which was triggered by the DME oxidation and prevailed as the amount of methane increased.

Yu et al. [143] used large eddy simulation (LES) to simulate ethanol HCCI combustion, in which the ethanol was port injected. The main scope of the study was to investigate the role of turbulence in the HCCI combustion process. The chemical mechanism used was that of Marinov [60]. The LES simulations were conducted for two different piston configurations, i.e. a disc shaped combustion chamber and a bowl in piston configuration, while maintaining the compression ratio. A grid consisting of $128 \times 128 \times 128$ mesh cells was used, with size about 1 mm in the radial direction and 0.32–1.5 mm in the axial direction for the square bowl-in-piston case and 0.075–1.3 mm for the disc-shaped combustion chamber case. This mesh size was of the order of Taylor microscale and at TDC close to the Kolmogorov microscale. Eight parallel processors and 48 h were necessary to yield a full cycle simulation for a four-stroke engine. The simulation results, which were validated against experiments, showed that the piston geometry affected the HCCI combustion process; the square bowl-in-piston design had a much slower combustion. Although the levels of turbulence in terms of the velocity components were similar, the temperature inhomogeneities were quite different between the two configurations. This was the reason for the longer combustion duration in the case of square bowl-in-piston design.

A similar study was later conducted by Joelsson et al. [144]. In this study, the researchers compared numerically and experimentally the ethanol HCCI combustion in a metal and an optical engine. The engines were essentially identical, the main difference being the piston material; a metal piston was used in the metal engine and a quartz piston head in the optical engine. It was expected that the quartz piston engine would operate at a higher piston temperature, since the quartz piston was air cooled, in contrast to the metal piston that was oil cooled. The scope of the study was to investigate the resulting thermal stratification differences and their effect on ethanol HCCI combustion. The same LES model was used in this study, as in the previous one. The expected difference in the piston temperatures was accounted for by increasing the piston surface temperature in the optical HCCI engine simulation. The simulation results showed that the two engines had minor differences in the induced turbulence field. However, the thermal stratification was much higher in the optical engine, due to the hotter quartz piston temperature and the lower intake temperature used in the optical engine. These factors prolonged the combustion duration, thereby decreasing the maximum pressure rise rate and the peak pressure.

Viggiano and Magi [145] used a multidimensional CFD model coupled with chemical kinetics to study ethanol HCCI combustion. The model used was the REC-200, which solves the 3D Reynolds averaged Navier–Stokes equations for transient, two-phase, turbulent, chemically reactive flows with sprays [146]. Turbulence was modeled with a two-equation k–ε model, and the heat and momentum fluxes were calculated using the wall function model of Launder and Spalding [147]. Combustion was modeled by coupling the turbulent flow to a detailed reaction mechanism. The approach used for the coupling was that of Kong and Reitz [148]. The influence of turbulence on the reaction rates was accounted for by multiplying the latter with a correction factor, which accounted for both the kinetic and turbulence timescales. The detailed reaction mechanism used was that of Saxena and Williams [59], which included 43 species and 235 reactions excluding NO_x formation reactions. The structured grid of the 1-degree sector considered, consisted of 26 cells in the radial direction. In the axial direction, the cell number varied from 48 at BDC to 8 at TDC by removing cell rows during compression. The grid resolution near the wall was kept at 0.2 mm. After the validation of the CFD model against experiments was accomplished, the researchers investigated the effect of turbulent timescale, turbulent diffusivity, initial and wall temperature, and equivalence ratio on HCCI combustion. They found that increasing the turbulent timescale induced a reduction to the combustion rate and decreased the pressure rise rate. Increasing the initial diffusivity delayed ignition and deteriorated the combustion rate. Inlet and wall temperature affected combustion in a similar manner, with the effect of inlet temperature being more pronounced; specifically, increasing T_{in} or T_{w} advanced ignition, enhanced combustion, and reduced CO emissions.

In Ref. [149] Liu and Karim examined numerically the effect of various operating parameters on hydrogen HCCI combustion. For the purposes of this investigation, the KIVA3 multi-dimension CFD code [121] was adopted with some modifications to make it suitable for modeling the turbulent combustion processes. Detailed chemical kinetics of hydrogen oxidation was implemented into the code, including 20 reactions with additional reactions involving nitrogen [71,72]. With this model, the researchers conducted a parametric study, the results of which showed that by increasing the swirl ratio heat transfer was enhanced, thereby reducing both the minimum and maximum temperature within the combustion chamber. As a result, ignition was retarded, combustion duration was prolonged, and the peak pressure and NO_x emissions were reduced. An increase in engine speed increased the heat loss rate due to the induced increase of the swirl ratio, but the heat losses were reduced because the time available for heat transfer was decreased. The calculations showed that there was an optimum engine speed in terms of indicated thermal efficiency. Initial temperature and compression ratio affected significantly the onset of combustion as well as the combustion duration.

Cotino and Jeanmart [150] studied numerically the running zone of ethyl acetate and compare it with the running zone of isooctane. Ethyl acetate was chosen, since it is a product of the acidogenic fermentation process used to produce biodiesel. This molecule was the basic compound and was used as a starting point to characterize a group of esters produced. The model used in the numerical study was the commercial CFD FLUENT code and the computational grid was obtained from the commercial software GAMBIT. The combustion mechanism used for ethyl acetate was a reduced one, consisting of 41 species and 203 reactions. This mechanism was derived from more detailed ones, namely the Gasnot et al. ethyl acetate submechanism [65], and the low carbon combustion mechanism of Miller and Melius [151]. Turbulence was modeled with the RNG k–ε model and the molecular mixing at the subgrid

level via the eddy dissipation model (EDC). Except for swirl motion, 3D effects were not included and an axisymmetric geometry was chosen, yielding 33,000 cells at IVC.

The model was validated against experimental results using isooctane as the fuel, and was subsequently used with ethyl acetate to determine the ethyl acetate HCCI operating limits (running zone) at 1200 rpm. The upper load limit was determined by the maximum pressure rise rate, which was set at 5 bar/CAD. The lower limit criterion implied combustion instability and was determined taking into account the combustion timing, the EGR rate, the sensitivity of the combustion on the initial temperature, the compatibility of the final and initial temperatures, and the CO emissions. The results of the study showed that the ethyl acetate had a similar running zone range as isooctane, but it was shifted toward higher loads. Moreover, ethyl acetate presented extended low temperature reactions compared to isooctane.

Um and Park [152] analyzed the chemical effects of biodiesel on combustion and emissions of an HCCI engine fueled with diesel/biodiesel blends. For this purpose, they used a modified version of the KIVA-3V code [121] in a 2D computational mesh, coupled with CHEMKIN chemistry solver [70]. The mechanism for biodiesel oxidation used was the one suggested by Brakora et al. [78], and was modified by Um and Park [153] to produce a reasonable ignition delay. The mechanism consisted of 156 reactions among 54 species. Since it was found that neat methyl butanoate was not suitable as a biodiesel surrogate, due to its high oxygen content, it was assumed that 1 mol of biodiesel consisted of 1 mol of methyl butanoate and 2 mol of n-heptane. Neat heptane was also used as a diesel surrogate. A NO_x mechanism, reduced from the Gas Research Institute (GRI) NO mechanism [84], was used for this study. It consisted of 12 reactions and 4 species (i.e., N, NO, NO_2, and N_2O). Moreover, a soot formation and oxidation model was incorporated, since rich mixtures with equivalence ratio up to 2.0 were used. The high equivalence ratio, which is impractical in actual HCCI engines, is justified considering the nature of the study, which was to examine the chemical properties of the biodiesel blends. Soot formation was calculated using a modified Hiroyasu model, which considers acetylene (C_2H_2) as a soot precursor [140], while soot oxidation was modeled using the Nagle–Strickland–Constable model [141].

The results of the study revealed that at stoichiometric equivalence ratio, increasing the biodiesel-to-diesel fuel ratio advanced ignition and decreased the total amount of heat released. This reduced the in-cylinder temperatures and induced a decrease in NO_x emissions with an increase in CO and HC. At richer mixtures ($\phi > 1.0$) increasing the biodiesel content increased CO, decreased NO_x and HC emissions, and decreased Soot emissions compared to neat diesel fuel operation. Below stoichiometric conditions ($\phi < 1.0$) CO and HC were formed in the cases where peak cycle temperatures were below 1400 K, NO_x was produced at peak temperatures higher than 1800 K, while Soot emissions were minimal. At rich mixtures significant amounts of CO and HC emissions were observed for most cases and soot emissions, which were higher for neat diesel, peaking in the cases with a peak cycle temperature of 1600 K. The NO_x and CO emission maps, i.e. equivalence ratio versus peak temperature maps, were similar for the diesel fuel and biodiesel cases.

6. Conclusions

Chemical kinetics are an essential part of biofueled HCCI combustion modeling, owing to the nature of HCCI combustion and the diversity of the biofuels' molecular structure. The development of chemical reaction mechanisms is an active research area, from which biofuel HCCI research can benefit. Efforts should be focused on the consistency of the various mechanisms developed for use in HCCI engines. Special care should be exercised on the selection of a chemical mechanism, depending on the conditions under which its validation was conducted. These conditions are preferably high pressure and low equivalence ratio, since such conditions are encountered in HCCI combustion. It would also be advisable to implement more than one chemical mechanism for the same biofuel in any HCCI simulation model, and compare the results. This helps to avoid reaching conclusions (e.g. on autoignition, or emissions formation), which are the result of the specific chemical mechanism used rather than the HCCI combustion process.

Single-zone models for biofuel HCCI combustion are very useful in identifying reaction paths and dominant chemical species during combustion. They have been used to provide insight into the behavior of various biofuels and blends thereof, and to validate the corresponding combustion mechanisms versus experiments or other more detailed mechanisms. Owing to the zero dimensional nature of the single-zone models, they have been used mainly to provide insight into the autoignition properties of the fuel and the formation of NO_x emissions. Single-zone models also provide an indication on the effect of various configurations, such as negative valve overlap, heavy EGR, fuel reforming, etc., on biofuel HCCI combustion.

Multi-zone models with their added feature of accounting for mixture thermal and fuel stratification, provide better and more realistic estimates on combustion duration, peak combustion pressure and emissions formation. Multi-zone models for biofuel HCCI combustion have been used to study the effect of various biofuels and their blends on the in-cylinder thermal stratification, combustion duration, emissions formation, and the overall performance. Not only can they provide an insight into the formation of CO and HC emissions, but also to the specific species formed and consumed in the low temperature regions of the combustion chamber, thereby indicating the species expected to be found in the exhaust of a HCCI engine. This is an important feature, since the composition of HC emissions can vary substantially in the case of biofuels, due to their non-conventional molecular structure.

Multi-dimensional models provide an even higher spatial resolution of the combustion chamber than the multi-zone ones. Gas flow during the gas exchange process or within the combustion chamber can be modeled in more detail, providing a more realistic spatial resolution of the species evolution during combustion. Moreover, mass flow between hot and cold regions is described in detail, providing an insight into the emissions formation process. Especially in the case of direct injection biofueled HCCI combustion, the physical properties of the fuel must be described in detail; properties such as viscosity, volatility, etc., are essential to describe the evolution of the fuel spray into the combustion chamber. The importance of these properties cannot be overemphasized, since the spray evolution will determine not only the fuel stratification within the combustion chamber but also the fuel impingement on the cylinder liner or the piston crown. The description of the physicochemical properties of biofuels is an active area of research, which is bound to be further advanced.

References

[1] Energy Statistics, Eurostat. http://epp.eurostat.ec.europa.eu/portal/page/portal/energy/data/database [accessed on 31.10.11].

[2] Escobar JC, Lora ES, Venturini OJ, Yáñez EE, Castillo EF, Almazan O. Biofuels: environment, technology and food security. Renew Sust Energy Rev 2009;13:1275–87.

[3] BP Statistical Review of World Energy, June 2010, http://www.bp.com/sectiongenericarticle.do?categoryId=9033088&contentId=7060602 [accessed on 1.6.11].

[4] Cherubini F, Bird ND, Cowie A, Jungmeier G, Schlamadinger B, Woess-Gallasch S. Energy- and greenhouse gas-based LCA of biofuel and bioenergy systems: key issues, ranges and recommendations. Resour Conserv Recycl 2009;53:434–47.

[5] Food and Agriculture Organization of the United Nations. http://www.fao.org/docrep/012/al390e/al390e00.pdf [accessed on 1.6.10, also in:

The State of Food Insecurity in the World, 2010, http://www.fao.org/docrep/013/i1683e/i1683e.pdf].
[6] http://esa.un.org/unpd/wpp/Excel-Data/population.htm [accessed on 1.6.10].
[7] Naik SN, Goud VV, Rout PK, Dalai AK. Production of first and second generation biofuels: a comprehensive review. Renew Sust Energy Rev 2010;14:578–97.
[8] Rakopoulos DC, Rakopoulos CD, Papagiannakis RG, Kyritsis DC. Combustion heat release analysis of ethanol or n-butanol diesel fuel blends in heavy-duty DI diesel engine. Fuel 2011;90:1855–67.
[9] Rakopoulos CD, Rakopoulos DC, Giakoumis EG, Dimaratos AM. Investigation of the combustion of neat cottonseed oil or its neat bio-diesel in a HSDI diesel engine by experimental heat release and statistical analyses. Fuel 2010;89:3814–26.
[10] Rakopoulos DC, Rakopoulos CD, Giakoumis EG, Papagiannakis RG, Kyritsis DC. Experimental-stochastic investigation of the combustion cyclic variability in HSDI diesel engine using ethanol–diesel fuel blends. Fuel 2008;87:1478–91.
[11] Rakopoulos CD, Antonopoulos KA, Rakopoulos DC, Hountalas DT. Multi-zone modeling of combustion and emissions formation in DI diesel engine operating on ethanol–diesel fuel blends. Energy Convers Manage 2008;49:625–43.
[12] Rakopoulos CD, Antonopoulos KA, Rakopoulos DC. Experimental heat release analysis and emissions of a HSDI diesel engine fueled with ethanol–diesel fuel blends. Energy 2007;32:1791–808.
[13] Rakopoulos CD, Antonopoulos KA, Rakopoulos DC. Development and application of multi-zone model for combustion and pollutants formation in direct injection diesel engine running with vegetable oil or its bio-diesel. Energy Convers Manage 2007;48:1881–901.
[14] Rakopoulos CD, Antonopoulos KA, Rakopoulos DC. Multi-zone modeling of diesel engine fuel spray development with vegetable oil, bio-diesel or diesel fuels. Energy Convers Manage 2006;47:1550–73.
[15] Rakopoulos CD, Rakopoulos DC, Giakoumis EG, Kyritsis DC. The combustion of n-butanol/diesel fuel blends and its cyclic variability in a DI diesel engine. Proc Inst Mech Eng Part A: J Power Energy 2011;225:289–308.
[16] Arcoumanis C, Bae C, Crookes R, Kinoshita E. The potential of di-methyl ether (DME) as an alternative fuel for compression-ignition engines: a review. Fuel 2008;87:1014–30.
[17] Szybist JP, Song J, Alam M, Boehman AL. Biodiesel combustion, emissions and emission control. Fuel Process Technol 2007;88:679–91.
[18] Rakopoulos CD, Kosmadakis GM, Demuynck J, De Paepe M, Verhelst S. A combined experimental and numerical study of thermal processes, performance and nitric oxide emissions in a hydrogen-fueled spark-ignition engine. Int J Hydrogen Energy 2011;36:5163–80.
[19] Rakopoulos CD, Kosmadakis GM, Pariotis EG. Evaluation of a combustion model for the simulation of hydrogen spark-ignition engines using a CFD code. Int J Hydrogen Energy 2010;35:12545–60.
[20] Rakopoulos CD, Michos CN. Generation of combustion irreversibilities in a spark ignition engine under biogas–hydrogen mixtures fueling. Int J Hydrogen Energy 2009;34:4422–37.
[21] Ji C, Liang C, Wang S. Investigation on combustion and emissions of DME gasoline mixtures in a spark-ignition engine. Fuel 2011;90:1133–8.
[22] Alkidas AC. Combustion advancements in gasoline engines. Energy Convers Manage 2008;48:2751–61.
[23] Yao M, Zheng Z, Liu H. Progress and recent trends in homogeneous charge compression ignition (HCCI) engines. Prog Energy Combust Sci 2009;35:398–437.
[24] Stanglemaier RH, Roberts CE. Homogeneous Charge Compression Ignition (HCCI): benefits, compromises and future engine applications, SAE paper no. 1999-01-3682; 1999.
[25] Lu X, Han D, Huang Z. Fuel design and management for the control of advanced compression-ignition combustion modes. Prog Energy Combust Sci 2011;37:741–83.
[26] Olsson J-O, Tunestål P, Johansson B. Closed-loop control of an HCCI engine, SAE paper no. 2001-01-1031; 2001.
[27] Antunes JMG, Mikalsen R, Roskilly AP. An investigation of hydrogen-fuelled HCCI engine performance and operation. Int J Hydrogen Energy 2008;33:5823–8.
[28] Christensen M, Einewall P, Johansson B. Homogeneous charge compression ignition (hcci) using isooctane, ethanol and natural gas—a comparison with spark-ignition operation, SAE paper no. 972874; 1997.
[29] Christensen M, Johansson B, Amneus PJH, Mauss F. Supercharged homogeneous charge compression ignition, SAE paper no. 980787; 1998.
[30] Yap D, Megaritis A. Applying forced induction to bioethanol HCCI operation with residual gas trapping. Energy Fuels 2005;19:1812–21.
[31] Megaritis A, Yap D, Wyszynski ML. Effect of inlet valve timing and water blending on bioethanol HCCI combustion using forced induction and residual gas trapping. Fuel 2008;87:732–9.
[32] Tsolakis A, Megaritis A, Yap D. Application of exhaust gas fuel reforming in diesel and homogeneous charge compression ignition (HCCI) engines fuelled with biofuels. Energy 2008;33:462–70.
[33] Manente V, Tunestal P, Johansson B. Influence of the wall temperature and combustion chamber geometry on the performance and emissions of a mini HCCI engine fuelled with DEE, SAE paper no. 2008-01-0008; 2008.
[34] Shudo T, Ono Y. HCCI Combustion of hydrogen, carbon monoxide and dimethyl ether, SAE paper no. 2002-01-0112; 2002.
[35] Chen Z, Konno M, Oguma M, Yanai T. Experimental study of CI natural-gas/DME homogeneous charge engine, SAE paper no. 2000-01-0329; 2000.
[36] Zheng ZQ, Yao MF, Chen Z, Zhang B. Experimental study on HCCI combustion of dimethyl ether (DME)/methanol dual fuel, SAE paper no. 2004-01-2993; 2004.
[37] Jothi NKM, Nagarajan G, Renganarayanan S. Experimental studies on homogeneous charge CI engine fueled with LPG using DEE as an ignition enhancer. Renew Energy 2007;32:1581–93.
[38] Szybist JP, McFarlane J, Bunting BG. Comparison of simulated and experimental combustion of biodiesel blends in a single cylinder diesel HCCI engine, SAE paper no. 2007-01-4010; 2007.
[39] Jia M, Xie M. A chemical kinetics model of iso-octane oxidation for HCCI engines. Fuel 2006;85:2593–604.
[40] Komninos NP, Rakopoulos CD. Numerical investigation into the formation of co and oxygenated and nonoxygenated hydrocarbon emissions from isooctane- and ethanol-fueled HCCI engines. Energy Fuels 2010;24:1655–67.
[41] Dagaut P, Togbé C. Experimental and modeling study of the kinetics of oxidation of butanol–n-heptane mixtures in a jet-stirred reactor. Energy Fuels 2009;23:3527–35.
[42] Black G, Curran HJ, Pichon S, Simmie JM, Zhukov V. Bio-butanol: combustion properties and detailed chemical kinetic modeling. Combust Flame 2010;157:363–73. http://c3.nuigalway.ie/biobutanol.html.
[43] Dagaut P, Togbé C. Oxidation kinetics of butanol–gasoline surrogate mixtures in a jet-stirred reactor: experimental and modeling study. Fuel 2008;87:3313–21.
[44] Saisirirat P, Togbé C, Chanchaona S, Foucher F, Mounaim-Rousselle C, Dagaut P. Auto-ignition and combustion characteristics in HCCI and JSR using 1-butanol/n-heptane and ethanol/n-heptane blends. Proc Combust Inst 2011;33:3007–14.
[45] Mack JH, Dibble RW, Buchholz BA, Flowers DL. The effect of the di-tertiary butyl peroxide (DTBP) additive on HCCI combustion of fuel blends of ethanol and diethyl ether, SAE paper no. 2005-01-2135; 2005.
[46] Yasunaga K, Simmie JM, Curran HJ, Koike T, Takahashi O, Kuraguchi Y, et al. Detailed chemical kinetic mechanisms of ethyl methyl, diethyl, methyl tert-butyl and ethyl tert-butyl ethers: The importance of unimolecular elimination reactions. Combust Flame 2011;158:1032–6. http://c3.nuigalway.ie/ethers.html.
[47] Yamada H. Simplified oxidation mechanism of DME applicable for compression ignition, SAE paper no. 2003-01-1819; 2003.
[48] Yao MF, Qin J, Zheng ZQ. Numerical study of the combustion mechanism of a homogeneous charge compression ignition engine fuelled with dimethyl ether and methane, with a detailed kinetics model. Part 1: the reaction kinetics of dimethyl ether. Proc Inst Mech Eng Part D: J Automob Eng 2005;219:1213–23.
[49] Liang X, Yao MF, Zheng ZQ. Numerical study on the mechanism of low temperature reaction of DME/methanol HCCI combustion. J Combust Sci Technol 2005;11:149–54 (in Chinese).
[50] Liang X. Numerical study on HCCI combustion of DME/MEOH dual fuels. Master's Dissertation, Tianjin University, Tianjin, China, 2005.
[51] Kim H, Cho S, Min K, Reduced chemical kinetic model of DME for HCCI combustion, SAE paper no. 2003-01-1822 (JSAE 20030263); 2003.
[52] Curran HJ, Pitz WJ, Marinov NM, Westbrook CK, Dagaut P, Boettner J-C, et al. A wide range modeling study of dimethyl ether oxidation. Int J Chem Kinet 1998;30:229–41.
[53] Fischer SL, Dryer FL, Curran HJ. The reaction kinetics of dimethyl ether. I: High-temperature pyrolysis and oxidation in flow reactors. Int J Chem Kinet 2000;32:713–40.
[54] Curran HJ, Fischer SL, Dryer FL. The reaction kinetics of dimethyl ether. II: Low-temperature oxidation in flow reactors. Int J Chem Kinet 2000;32:741–59.
[55] Kaiser EW, Wallington TJ, Hurley MD, Platz J, Curran HJ, Pitz WJ, et al. Experimental and modeling study of premixed atmospheric-pressure dimethyl ether–air flames. J Phys Chem A 2000;104:8194–206, available at https://www-pls.llnl.gov/?url=science_and_technology-chemistry-combustion-dme [accessed on 8.3.11].
[56] Chun-lan M, Yu-sheng Z, Yu S, Jian H, Hai-ying S. Experimental and numerical study on emission in an HCCI Engine operated with neat dimethyl ether, SAE paper no. 2007-01-1888; 2007.
[57] Röhl O, Peters N. A reduced mechanism for ethanol oxidation. In: European Combustion Meeting. 2009.
[58] Li J, Kazakov A, Chaos M, Dryer FL. Chemical kinetics of ethanol oxidation, Paper no. C26, Fifth US Combustion Meeting, San Diego; 2007.
[59] Saxena P, Williams FA. Numerical and experimental studies of ethanol flames. Proc Combust Inst 2007;31:1149–56.
[60] Marinov NM. A detailed chemical kinetic model for high temperature ethanol oxidation. Int J Chem Kinet 1999;31:183–220.
[61] Curran H, Serinyel Z, Metalcafe W. Combustion Chemistry Center at NUI Galway, Ireland; 2009. Personal communication with M. Sjöberg, J.E. Dec of the Sandia National Labs.
[62] Mosbach S, Kraft M, Bhave A, Mauss F, Mack JH, Dibble RW. Simulating a homogeneous charge compression ignition engine fuelled with a dee/etoh blend, SAE paper no 2006-01-1362; 2006.
[63] Dagaut P, Togbé C. Experimental and modeling study of the kinetics of oxidation of ethanol–n-heptane mixtures in a jet-stirred reactor. Fuel 2010;89:280–6.
[64] Dagaut P, Togbé C. Experimental and modeling study of the kinetics of oxidation of ethanol–gasoline surrogate mixtures (E85 surrogate) in a jet-stirred reactor. Energy Fuels 2008;22:3499–505.

[65] Gasnot L, Decottignies V, Pauwels JF. Kinetics modelling of ethyl acetate oxidation in flame conditions. Fuel 2005;84:505–18.
[66] Mueller MA, Kim TJ, Yetter RA, Dryer FL. Flow reactor studies and kinetic modeling of the H_2/O_2 reaction. Int J Chem Kinet 1999;31:113–25.
[67] Marinov NM, Westbrook CK, Pitz WJ. Detailed and global chemical kinetics model for hydrogen. In: Chan SH, editor. Trasnport Phenomena in Combustion. Washington, DC: Taylor and Francis; 1996. p. 118–41.
[68] O'Connaire M, Curran HJ, Simmie JM, Pitz WJ, Westbrook CK. A comprehensive modeling study of hydrogen oxidation. Int J Chem Kinet 2004;36:603–22.
[69] Westbrook CK, Dryer FL. Chemical kinetic modeling of hydrocarbon combustion. Prog Energy Combust Sci 1984;10:1–57.
[70] Kee RJ, Rupley FM, Miller JA. Chemkin-II: A FORTRAN chemical kinetics package for the analysis of gas-phase chemical kinetics, Sandia National Labs Report SAND89-8009B; 1991.
[71] Li H, Karim GA. Knock in spark ignition hydrogen engines. Int J Hydrogen Energy 2004;29:859–65.
[72] Liu KC. An experimental and analytical investigation into the combustion characteristics of HCCI and dual fuel engines with pilot injection, PhD thesis in Mechanical Engineering, University of Calgary, Canada; 2006.
[73] Li J, Zhao Z, Kasakov A, Chaos M, Dryer FL, Scire JJ. A comprehensive kinetic mechanism for CO, CH_2O, and CH_3OH combustion. Int J Chem Kinet 2007;39:109–36.
[74] Held TJ, Dryer FL. A comprehensive mechanism for methanol oxidation. Int J Chem Kinet 1998;30:805–30.
[75] Westbrook CK, Dryer FL. A comprehensive mechanism for methanol oxidation. Combust Sci Technol 1979;20:125–40.
[76] Westbrook CK, Dryer FL. Prediction of laminar flame properties of methanol-air mixtures. Combust Flame 1980;37:171–92.
[77] Lindstedt RP, Meyer MP. A dimensionally reduced reaction mechanism for methanol oxidation. Proc Combust Inst 2002;29:1395–402.
[78] Brakora JL, Ra Y, Reitz RD, McFarlane J, Daw SC. Development and validation of a reduced reaction mechanism for biodiesel-fueled engine simulations. SAE Int J Fuels Lubr 2008;1:675–702 (SAE paper no. 2008-01-1378).
[79] Dooley S, Curran HJ, Simmie JM. Autoignition measurements and a validated kinetic model for the biodiesel surrogate, methyl butanoate. Combust Flame 2008;153:2–32.
[80] Gaïl S, Thomson MJ, Sarathy SM, Syed SA, Dagaut P, Diévart P, et al. A wide-ranging kinetic modeling study of methyl butanoate combustion. Proc Combust Inst 2007;31:305–11.
[81] Herbinet O, Pitz WJ, Westbrook CK. Detailed chemical kinetic oxidation mechanism for a biodiesel surrogate. Combust Flame 2008;154:507–28.
[82] Bowman CT. Control of combustion-generated nitrogen oxide emissions. In: Proc. of the 24th Symposium (International) on Combustion, The Combustion Institute. 1992. p. 859–78.
[83] Lavoie GA, Heywood JB, Keck JC. Experimental and theoretical investigation of nitric oxide formation in internal combustion engines. Combust Sci Technol 1970;1:313–26.
[84] Smith GP, Golden DM, Frenklach M, Moriarty NW, Eiteneer B, Goldenberg M, et al. GRI-Mech v.3.0; 2011. http://www.me.berkeley.edu/gri_mech/.
[85] Marinov NM, Pitz WJ, Westbrook CK, Hori M, Matsunaga N. An experimental and kinetic calculation of the promotion effect of hydrocarbons on the NO–NO_2 conversion in a flow reactor. Proc Combust Inst 1998;27: 389–96.
[86] Isooctane oxidation mechanism; 2003, http://www.tfd.chalmers.se/~valeri/MECH.html.
[87] Yoshikawa T, Reitz RD. Development of an improved NO_x reaction mechanism for low temperature diesel combustion modeling, SAE paper no. 2008-01-2413; 2008.
[88] Fiveland SB, Assanis DN. A four-stroke homogeneous charge compression ignition engine simulation for combustion and performance studies, SAE paper no. 2000-01-0332; 2000.
[89] Goldsborough SS, Van Blarigan P. A numerical study of a free piston IC engine operating on homogeneous charge compression ignition combustion, SAE paper no. 1999-01-0619; 1999.
[90] Lund CM. HCT: a general computer program for calculating time-dependent phenomena involving one-dimensional hydrodynamics, transport and detailed chemical kinetics, Lawrence Livermore National Laboratory Report UCRL-52504, rev; 1995.
[91] Woschni G. A universally applicable equation for the instantaneous heat transfer coefficient in the internal combustion engine, SAE paper no. 670931; 1967.
[92] Ng CKW, Thomson MJ. A computational study of the effect of fuel reforming, EGR and initial temperature on lean ethanol HCCI combustion, SAE paper no. 2004-01-0556; 2004.
[93] Martinez-Frias J, Aceves SM, Flowers DL. Improving ethanol life cycle energy efficiency by direct utilization of wet ethanol in HCCI engines. Trans ASME J Energy Resour Technol 2007;129:332–7.
[94] http://www.reactiondesign.com; 2011.
[95] Szybist JP. Fuel-specific effect of exhaust gas residuals on HCCI combustion: a modeling study, SAE paper no. 2008-01-2402; 2008.
[96] Yang D, Wang Z, Wang J-X, Shuai S. Experiment and chemical kinetics analysis of active atmosphere with different fuels in HCCI combustion. Energy Fuels 2010;24:4872–8.
[97] Hoffman SR, Abraham J. A comparative study of n-heptane, methyl decanoate, and dimethyl ether combustion characteristics under homogeneous-charge compression–ignition engine conditions. Fuel 2009;88:1099–108.
[98] Brakora JL, Reitz RD. Investigation of NO_x predictions from biodiesel-fueled HCCI engine simulations using a reduced kinetic mechanism, SAE paper no. 2010-01-0577; 2010.
[99] Curran HJ, Gaffuri P, Pitz PJ, Westbrook CK. A comprehensive modeling study of n-heptane oxidation. Combust Flame 1998;114:149–77.
[100] Saisirirat P, Foucher F, Chanchaona S, Mounaïm-Rousselle C. Spectroscopic measurements of low-temperature heat release for homogeneous combustion compression ignition (HCCI) n-heptane/alcohol mixture combustion. Energy Fuels 2010;24:5404–9.
[101] Mack JH, Flowers DL, Buchholz BA, Dibble RW. Investigation of HCCI combustion of diethyl ether and ethanol mixtures using carbon 14 tracing and numerical simulations. Proc Combust Inst 2005;30:2693–700.
[102] Iizuka Y, Surianarayanan M. Comprehensive kinetic model for adiabatic decomposition of di-tert-butyl peroxide using BatchCAD. Ind Eng Chem Res 2003;42:2987–95.
[103] Yao M, Zheng Z, Liang X. Numerical study on the chemical reaction kinetics of DME/methanol for HCCI combustion process, SAE paper no. 2006-01-1521; 2006.
[104] Yao M, Qin J, Zheng Z. Numerical study of the combustion mechanism of a homogeneous charge compression ignition engine fuelled with dimethyl ether and methane, with a detailed kinetics model. Part 2: the reaction kinetics of dimethyl ether and methane dual-fuel. Proc Inst Mech Eng Part D: J Automob Eng 2005;219:1225–36.
[105] Ogawa H, Miyamoto N, Kaneko N, Ando H. Combustion control and operating range expansion with direct injection of reaction suppressors in a premixed DME HCCI engine, SAE paper no. 2003-01-0746; 2003.
[106] Shudo T, Yamada H. Hydrogen as an ignition-controlling agent for HCCI combustion engine by suppressing the low-temperature oxidation. Int J Hydrogen Energy 2007;32:3066–72.
[107] Shudo T, Shima Y, Fujii T. Production of dimethyl ether and hydrogen by methanol reforming for an HCCI engine system with waste heat recovery–continuous control of fuel ignitability and utilization of exhaust gas heat. Int J Hydrogen Energy 2009;34:7638–47.
[108] Yamada H, Yoshii M, Tezaki A. Chemical mechanistic analysis of additive effects in homogeneous charge compression ignition of dimethyl ether. Proc Combust Inst 2005;30:2773–80.
[109] Heirmel JM, Coffee TP. The unimolecular ozone decomposition reaction. Combust Flame 1979;35:117–23.
[110] Komninos NP. Assessing the effect of mass transfer on the formation of HC and CO emissions in HCCI engines, using a multi-zone model. Energy Convers Manage 2009;50:1192–201.
[111] Noda T, Foster DE, A numerical study to control combustion duration of hydrogen-fueled HCCI by using multi-zone chemical kinetics simulation, SAE paper no. 2001-01-0250; 2001.
[112] Komninos NP, Hountalas DT, Rakopoulos CD. A parametric investigation of hydrogen HCCI combustion using a multi-zone model approach. Energy Convers Manage 2007;48:2934–41.
[113] Komninos NP, Rakopoulos CD. Comparison of a detailed and a reduced ethanol oxidation mechanism in HCCI combustion using a multi-zone model. Open Renew Energy J 2011;4:47–59.
[114] Annand WJD. Heat transfer in the cylinders of reciprocating internal combustion engines. Proc Inst Mech Eng 1963;177:973–90.
[115] Komninos NP. Modeling HCCI combustion: modification of a multi-zone model and comparison to experimental results at varying boost pressure. Appl Energy 2009;86:2141–51.
[116] Schofield K. The enigmatic mechanism of the flame ionization detector: Its overlooked implications for fossil fuel combustion modeling. Prog Energy Combust Sci 2008;34:330–50.
[117] Sjoberg M, Dec JE. Ethanol autoignition characteristics and HCCI performance for wide ranges of engine speed, load and boost, SAE paper no. 2010-01-0338; 2010.
[118] Sjoberg M, Dec JE. Effects of EGR and its constituents on HCCI autoignition of ethanol. Proc Combust Inst 2011;33:3031–8.
[119] Mehl M, Pitz WJ, Sjöberg M, Dec JE. Detailed kinetic modeling of low-temperature heat release for PRF fuels in an HCCI engine, SAE paper no. 2009-01-1806; 2009.
[120] Kim HJ, Park SH, Lee KS, Lee CS. A study of spray strategies on improvement of engine performance and emissions reduction characteristics in a DME fueled diesel engine. Energy 2011;36:1802–13.
[121] Amsden AA. KIVA-3V release 2. Improvement to KIVA-3V. Los Alamos National Laboratory, LA-UR-99-915; 1999.
[122] Teng H, McCandless JC, Schneyer JB, Thermochemical characteristics of dimethyl ether—an alternative fuel for compression-ignition engines, SAE paper no. 2001-01-0154; 2001.
[123] Teng H, McCandless JC, Schneyer JB. Viscosity and lubricity of (liquid) dimethyl ether e an alternative fuel for compression-ignition engines, SAE paper no. 2002-01-0862; 2002.
[124] Teng H, McCandless JC, Schneyer JB. Compression ignition delay (physical + chemical) of dimethyl ether e an alternative fuel for compression-ignition engines, SAE paper no. 2003-01-0759; 2003.
[125] Teng H, McCandless JC, Schneyer JB. Thermodynamic properties of dimethyl ether—an alternative fuel for compression-ignition engines, SAE paper no. 2004-01-0093; 2004.
[126] Teng H, McCandless JC. Comparative study of characteristics of diesel-fuel and dimethyl-ether sprays in the engine, SAE paper no. 2005-01-1723; 2005.

[127] Kong SC, Sun Y, Reitz RD. Modeling diesel spray flame lift-off, sooting tendency and NO_x emissions using detailed chemistry with phenomenological soot model. Trans ASME J Eng Gas Turb Power 2007;129:252–60.
[128] Beale JC, Reitz RD. Modeling spray atomization Kelvin–Helmholtz/Rayleigh–Taylor hybrid model. Atomiz Sprays 1999;9:623–50.
[129] Han Z, Reitz RD. Turbulence modeling of internal combustion engines using RNG ke3 models. Combust Sci Technol 1995;106:267–95.
[130] O'Rourke PJ, Amsden AA. A spray/wall interaction submodel for the KIVA-3 wall film model, SAE paper no. 2000-01-0271; 2000.
[131] Park SH, Kim HJ, Lee CS. Macroscopic spray characteristics and breakup performance of dimethyl ether (DME) fuel at high fuel temperatures and ambient conditions. Fuel 2010;89:3001–11.
[132] Kim HJ, Suh HK, Lee CS. Numerical and experimental study on the comparison between diesel and dimethyl ether (DME) spray behaviors according to combustion chamber shape. Energy Fuels 2008;22:2851–60.
[133] Chen Z, Yao M, Zheng Z, Zhang Q. Experimental and numerical study of methanol/dimethyl ether dual-fuel compound combustion. Energy Fuels 2009;23:2719–30.
[134] AVL FIRE UsersGuide, version 8.4, AVL LIST GmbH; 2005.
[135] AVL FIRE Spray, version 8.4, AVL LIST GmbH; 2005.
[136] Han ZW, Reitz RD. A temperature wall function formulation for variable-density turbulent flows with application to engine convective heat transfer modeling. Int J Heat Mass Transfer 1997;40:613–25.
[137] Yao M, Huang C, Zheng Z. Multidimensional numerical simulation on dimethyl ether/methanol dual-fuel homogeneous charge compression ignition (HCCI) engine combustion and emission processes. Energy Fuels 2007;21:812–21.
[138] Huang C, Yao M, Lu X, Huang Z. Study of dimethyl ether homogeneous charge compression ignition combustion process using a multi-dimensional computational fluid dynamics model. Int J Therm Sci 2009;48:1814–22.
[139] Park SW. Numerical study on optimal operating conditions of homogeneous charge compression ignition engines fueled with dimethyl ether and n-heptane. Energy Fuels 2009;23:3909–18.
[140] Kong S-C, Sun Y, Reitz RD. Modeling diesel spray flame liftoff, sooting tendency, and NO_x emissions using detailed chemistry with phenomenological soot model. Trans ASME J Eng Gas Turb Power 2007;129:245–51.
[141] Han Z, Uludogan A, Hampson GJ, Reitz RD. Mechanism of soot and NO_x emission reduction using multiple-injection in a diesel engine, SAE paper no. 960633; 1996.
[142] Kong S-C. A study of natural gas/DME combustion in HCCI engines using CFD with detailed chemical kinetics. Fuel 2007;86:1483–9.
[143] Yu RX, Bai XS, Vressner A, Hultqvist A, Johansson B, Olofsson J, et al. Effect of turbulence on HCCI combustion, SAE paper no. 2007-01-0183; 2007.
[144] Joelsson T, Yu R, Bai XS, Vressner A, Johansson B. Large eddy simulation and experiments of the auto-ignition process of lean ethanol/air mixture in HCCI engines, SAE paper no. 2008-01-1668; 2008.
[145] Viggiano A, Magi V. Multidimensional simulation of ethanol HCCI engines, SAE paper no. 2009-24-0031; 2009.
[146] Magi V. REC-2000: A multidimensional code for engines, Engine research laboratory report, School of Mechanical Engineering, Purdue University; 2000.
[147] Launder BE, Spalding DB. The numerical computations of turbulent flows. Comput Method Appl Mech 1974;3:269–89.
[148] Kong S-C, Reitz RD. Numerical study of premixed HCCI engine combustion and its sensitivity to computational mesh and model uncertainties. Combust Theor Model 2002;7:417–33.
[149] Liu C, Karim GA. A simulation of the combustion of hydrogen in HCCI engines using a 3D model with detailed chemical kinetics. Int J Hydrogen Energy 2008;33:3863–75.
[150] Contino F, Jeanmart H. Study of the HCCI running zone using ethyl acetate, SAE paper no. 2009-01-0297; 2009.
[151] Miller JA, Melius CF. Kinetic and thermodynamic issues in the formation of aromatic compounds in flames of aliphatic fuels. Combust Flame 1992;91:21–39.
[152] Um S, Park SW. Numerical study on combustion and emission characteristics of homogeneous charge compression ignition engines fueled with biodiesel. Energy Fuels 2010;24:916–27.
[153] Um S, Park SW. Modeling effect of the biodiesel mixing ratio on combustion and emission characteristics using a reduced mechanism of methyl butanoate. Fuel 2010;89:1415–21.